Strongly nonlinear dynamics of electrolytes in large ac voltages

Laurits Højgaard Olesen,[1,2] Martin Z. Bazant,[3,4] and Henrik Bruus[1]
[1]*Department of Micro- and Nanotechnology, Technical University of Denmark, DTU Nanotech Building 345 East, DK-2800 Kongens Lyngby, Denmark*
[2]*Novo Nordisk A/S, Brennum Park, DK-3400 Hillerød, Denmark*
[3]*Department of Chemical Engineering and Department of Mathematics, Massachusetts Institute of Technology, Cambridge, Massachusetts 02139, USA*
[4]*CNRS UMR Gulliver 7083, ESPCI, 10 rue Vauquelin, F-75005 Paris, France*
(Received 2 November 2009; revised manuscript received 12 May 2010; published 2 July 2010)

We study the response of a model microelectrochemical cell to a large ac voltage of frequency comparable to the inverse cell relaxation time. To bring out the basic physics, we consider the simplest possible model of a symmetric binary electrolyte confined between parallel-plate blocking electrodes, ignoring any transverse instability or fluid flow. We analyze the resulting one-dimensional problem by matched asymptotic expansions in the limit of thin double layers and extend previous work into the strongly nonlinear regime, which is characterized by two features—significant salt depletion in the electrolyte near the electrodes and, at very large voltage, the breakdown of the quasiequilibrium structure of the double layers. The former leads to the prediction of "ac capacitive desalination" since there is a time-averaged transfer of salt from the bulk to the double layers, via oscillating diffusion layers. The latter is associated with transient diffusion limitation, which drives the formation and collapse of space-charge layers, even in the absence of any net Faradaic current through the cell. We also predict that steric effects of finite ion sizes (going beyond dilute-solution theory) act to suppress the strongly nonlinear regime in the limit of concentrated electrolytes, ionic liquids, and molten salts. Beyond the model problem, our reduced equations for thin double layers, based on uniformly valid matched asymptotic expansions, provide a useful mathematical framework to describe additional nonlinear responses to large ac voltages, such as Faradaic reactions, electro-osmotic instabilities, and induced-charge electrokinetic phenomena.

DOI: 10.1103/PhysRevE.82.011501 PACS number(s): 82.45.Gj, 82.45.Mp, 66.10.−x

I. INTRODUCTION

Time-dependent voltages are applied to electrolytes in many different fields, and theoretical models to interpret the results have been developed for over a century [1]. Current applications include energy storage in electrochemical systems (e.g., supercapacitors [2–4] and high-rate batteries [5–7]), flow control in microfluidics (e.g., ac electro-osmotic [8–18] and electrothermal [19,20] flows), particle handling in colloidal materials (e.g., dielectrophoresis [21,22] and induced-charge electrophoresis [23–26]), and cellular and molecular manipulation in the biological systems (e.g., electroporation [27–29], cell trapping [22,30,31], and biomolecular sensing [32–36]).

In many cases, periodic voltages are used to drive alternating current (ac) to eliminate any net linear response, such as direct current or electro-osmotic flow. The most common application of ac forcing is in impedance spectroscopy, long used to characterize electrochemical interfaces [37]. The current response to a small sinusoidal voltage is fitted to an electrical circuit model, where the interface acts as an impedance in series with a bulk resistance [38–40]. The characteristic frequency for double-layer charging is then the inverse "*RC* time" of the equivalent circuit [1]. Circuit models are also used to describe electrochemical response in much more complicated situations, such as composite porous electrodes [3,4], microelectrode arrays [9,10,14,16,31], and biological tissues [27,28].

Circuit models can be derived from underlying ion-transport equations by considering the joint limit of thin double layers ($\epsilon=\lambda_D/L\ll 1$, where λ_D is the Debye-Hückel screening length and L is the geometrical scale) and small voltages ($V\ll kT/e$, where V is the amplitude of the applied voltage and kT/e is the thermal voltage) [1]. From a mathematical point of view, this can be done systematically starting from the Poisson-Nernst-Planck (PNP) equations by asymptotic boundary-layer analysis, which was introduced to electrochemistry in the 1960s to justify the thin-double-layer approximation [41–45]. The joint asymptotic limit of thin double layers and large voltages, which is mathematically more challenging and physically more complex, has also been analyzed under conditions of steady direct current (dc). At sufficiently large *steady* dc currents, exceeding diffusion limitation, a variety of exotic effects arise, such as the expansion of the double layer into an extended nonequilibrium space-charge layer [46–48] and electrohydrodynamic instability due to second-kind electro-osmotic (EO) flows [49–51]. Clearly, such effects cannot be captured by classical circuit models, but they continue to be used in dynamical situations, even with large voltages, for lack of a simple mathematical alternative.

The *transient* electrochemical response to a large dc voltage (without Faradaic reactions) has only been analyzed quite recently [1,52–55]. Even in the limit of thin double layers, the large voltage leads to a number of new dynamical effects not captured by circuit models. Additional time scales enter the problem, other than the fundamental *RC* time scale (which can be expressed as $\lambda_D L/D$, where D is the ion diffusivity [1]). In the simplest one-dimensional (1D) problem with parallel-plate, blocking electrodes, overcharging of the

double-layer "capacitors" leads to net adsorption of neutral salt from the bulk, regardless of the polarity of the diffuse-layer voltage [1]. This process is coupled to slow diffusive relaxation of the bulk concentration (at the time scale L^2/D), which leads to transient concentration polarization and thus breakdown of Ohm's law for the bulk "resistor." In higher dimensions, large applied voltages also trigger surface transport of ions through the double layers [56], which completes flux loops driven by bulk concentration gradients in and out of the double layers [52].

At large voltages, another important consideration is the breakdown of dilute-solution theory [57,58], including the Poisson-Boltzmann (PB) model of the double layer [53] and, more generally, the PNP equations from which it is derived [54]. These classical models are strictly valid only for a dilute solution of pointlike ions; but, even in a very dilute bulk solution, the application of a large voltage can lead to the crowding of counterions near a highly charged electrode. Among many possible modifications of the PB model, one must at least account for the finite sizes of ions and solvent molecules. This generally leads to the formation of a condensed layer of crowded ions, anticipated by Stern [59] and first described 1942 by Bikerman [60], whose simple modified PB (MPB) model has been rederived several times in different contexts [61–67]. As perhaps first predicted by Freise in 1952 [68], the widening of the condensed layer generally causes the diffuse-layer differential capacitance to decay at large voltages—the opposite trend from PB theory, which allows ions to pile up with exponentially diverging concentration. This has major implications for the dynamics of electrolytes at large voltages [53,57,58,69] as well as ionic liquids and molten salts [70–73] (where crowding dominates in the absence of a solvent). In electrolytes, for the same reason, steric constraints also greatly reduce salt adsorption and surface conduction compared to PB theory by limiting the charge density of the double layer [53,56]. All of these conclusions are independent of the model for steric effects on the chemical potential of ions in a concentrated solution [57,74] and can be extended to more general situations, without assuming thin double layers, by deriving modified PNP (MPNP) equations [54].

A number of recent developments provide further motivation for our work. In a recent paper [55], Beunis *et al.* revisited the problem of a suddenly applied large dc voltage in a blocking cell and studied the formation of *transient space-charge layers* at very large voltage, a possibility predicted in Ref. [1] and analyzed preliminarily in Ref. [75]. Two recent papers, by Suh and Kang [76,77], analyze the weakly nonlinear response of an electrolyte to an ac voltage, which is relevant for many of the experimental situations described above. By coupling weakly nonlinear charge relaxation to fluid flow, novel concentrated-solution effects can enter theory of induced-charge electrokinetic phenomena in large ac voltages [58]. In the context of electrodialysis membranes, it is well known that strongly nonlinear effects are important and can lead to electro-osmotic instability at the limiting current [49–51], but this possibility is just beginning to be explored experimentally using large ac voltages. Building on recent observations of salt depletion and electroconvection near microchannel and nanochannel junctions [78], the Rubinstein-Zaltzman instability has been demonstrated experimentally by applying low-frequency ac (square-wave) voltages to confine it to slowly oscillating boundary layers [79]. This experiment raises interesting theoretical questions about the periodic breakdown and restoration of the quasi-equilibrium structure of the double layer under strong ac forcing, which are a major focus of this paper.

In this work, we analyze the strongly nonlinear, time-dependent response of an electrolyte or ionic liquid to a large ac voltage. The imposition of a time scale (the ac period) is a significant complication compared to case of a sudden dc voltage, so we focus on the simplest geometry of parallel-plate blocking electrodes and ignore any transverse instability. Following Ref. [1], we analyze the resulting one-dimensional problem starting from the classical PNP equations and derive accurate asymptotic approximations for thin double layers. We also consider the MPNP equations of Ref. [54] to highlight steric effects under ac forcing. Using both PNP and MPNP models, we study the formation and collapse of transient space-charge layers at large voltages. While Beunis *et al.* [55] focused on the extreme case where the space-charge layer completely dominates the response at very large voltages (in sufficiently large systems and high salt concentrations), we aim to derive a reduced model that is uniformly valid for all voltages and all salt concentrations, ranging from dilute electrolytes to concentrated solutions. In spite of the mathematical complexity of these problems, our goal is to extract generic predictions and useful analytical approximations to aid in interpreting experimental data.

The paper is organized as follows. We begin in Sec. II by stating the mathematical problem, converting to dimensionless form, and showing full numerical solutions used to test our subsequent analytical approximations. In Sec. III we briefly go through the asymptotic analysis for double layers in quasiequilibrium, adapting the results of Ref. [1] concerning the transient dynamics, to our case of interest, namely, the steady-state response when an ac voltage with frequency around the inverse RC time is applied. In Secs. IV and V we study the dynamic response in the weakly and strongly nonlinear regimes, respectively, and also compare the strongly nonlinear asymptotic analysis to the full numerical solution. In Sec. VI we develop an asymptotic analysis for the case when the double layers are driven *out of quasiequilibrium* to form bulk space charge and also compare those results to the full numerical solution. Finally, in Sec. VII we summarize and briefly discuss extensions to higher dimensions, Faradaic currents, and nonlinear electro-osmotic flows, building on the initial study of Ref. [75], and we leave the reader with some open questions.

II. GOVERNING EQUATIONS

A. General models

In any continuum model, the transport of ions in the electrolyte is governed by a mass conservation law

$$\partial_t c_i = -\nabla \cdot \mathbf{F}_i, \tag{1}$$

where c_i is the local concentration of the ith ionic species, $\mathbf{F}_i$ is the flux, and we neglect any bulk reactions in the electro-

lyte which could produce or consume ions. Quite generally, in a concentrated solution, the flux can be expressed in terms of the gradient of the electrochemical potential μ_i as

$$\mathbf{F}_i = -\sum_j L_{ij} c_j \nabla \mu_j + \mathbf{u} c_i, \tag{2}$$

where the first term describes ion transport by diffusion and electromigration, L_{ij} is the Onsager mobility tensor, and the second term describes advection at the mean fluid velocity $\mathbf{u}$, as determined by momentum conservation. The mobility tensor is related to the diffusivity tensor by the Einstein relation $D_{ij}=kTL_{ij}$, where k is the Boltzmann constant and T is the absolute temperature, and is usually assumed to be diagonal, $L_{ij}=L_i\delta_{ij}$, although this can only be justified for a dilute solution—in a highly concentrated solution there may be significant off-diagonal elements [80,81].

For a dilute solution, the chemical potential μ_i takes the ideal form, with contributions from entropy and mean electrostatic energy,

$$\mu_i = kT \ln c_i + z_i e \phi, \tag{3}$$

where ϕ is the electrostatic potential, z_i is the ionic valence, and e is the electron charge. Equation (2) then reduces to the Nernst-Planck equation

$$\mathbf{F}_i = -D_i\left(\nabla c_i + \frac{z_i e}{kT} c_i \nabla \phi\right) + \mathbf{u} c_i. \tag{4}$$

In the usual mean-field approximation, the electrostatic potential is self-consistently determined by the charge density ρ through Poisson's equation

$$-\nabla \cdot (\varepsilon \nabla \phi) = \rho = \sum_i z_i e c_i, \tag{5}$$

where ε is the electrolyte permittivity, which we take to be constant. This completes the classical PNP equations, which underlie most of electrochemical transport theory. As noted above, the characteristic length scale in these equations (the Debye-Hückel screening length) is

$$\lambda_D = \sqrt{\frac{\varepsilon kT}{\sum_i c_i^* z_i^2 e^2}}. \tag{6}$$

where c_i^* is the nominal bulk concentration of the ith ionic species.

In the present work we focus on dilute electrolytes for which the nominal bulk salt concentration is small, seemingly within the range of applicability of the PNP equations. Even in a very dilute bulk solution, however, when a large external bias is placed on the electrodes in the system (only a few times kT/e), ions accumulate at the surface, and the dilute-solution approximation must break down [53,57,58]. Following Kilic *et al.* [54], we will solve modified (MPNP) equations based on the oldest and simplest approach to steric effects of ion crowding of Bikerman [60], which corresponds to the following model for the chemical potential in a binary $z:z$ electrolyte [54,74]:

$$\mu_\pm = kT \ln c_\pm \pm ze\phi - kT \ln(1 - c_+a^3 - c_-a^3), \tag{7}$$

where a is an effective molecular length scale. (For a history of this model and related concentrated-solution theories, see Ref. [58].) The correction term, which can be interpreted as an activity coefficient $f_i=\exp[(\mu_i-\mu_i^{\text{ideal}})/kT]$, is related to the entropy of the solvent molecules and imposes a maximum ion concentration $c_{\max}=a^{-3}$; it can be derived from the statistical mechanics of equal-sized ions and solvent molecules on a cubic lattice of spacing a in the continuum limit. In equilibrium, $\mu_\pm$ is constant, and the ions effectively obey Fermi-Dirac statistics, rather than classical Boltzmann statistics, due to the excluded volume effect [61–67,70].

We must emphasize that we consider this only a simple first approximation to model finite ion size. Bikerman's model, like other *mean-field local-density* theories, is known to provide a poor description of confined hard-sphere liquids, even in equilibrium. For example, it cannot capture two point correlation functions or density oscillations (layering) on the molecular scale a near a hard wall [82]. Strictly, imposing $c_{\max}=a^{-3}$ can be justified only if the ion concentrations are sufficiently smooth on the molecular scale, which may not be the case in the double layer close to the electrodes. Nevertheless, Bikerman's simple model does show the correct qualitative behavior of the double-layer capacitance at large voltage, and allows experimental data to be fitted well [58], which makes it a convenient (and analytically tractable) choice to study the impact of volume constraints on the system dynamics at large applied voltage.

For boundary conditions at the (blocking) electrodes, we assume no electrochemical reactions, so the normal ionic fluxes must vanish $\mathbf{n}\cdot\mathbf{F}_i=0$. To close the system, we follow many prior authors [1,10,11,16,45,83,84] and allow for a compact (Stern) layer or thin dielectric coating separating the electrode from the electrolyte with a constant "surface capacitance" per unit area C_S, which leads to a mixed boundary condition

$$C_S(V_{\text{ext}} - \phi) + \varepsilon \mathbf{n} \cdot \nabla \phi = 0. \tag{8}$$

Here, $\mathbf{n}$ is a surface normal pointing into the electrolyte, $C_S=\varepsilon_S/h_S$ can be ascribed to a surface coating of thickness h_S and dielectric constant ε_S, and $V_{\text{ext}}(t)$ is the external potential applied at the electrode.

For the present analysis we focus on a symmetric binary electrolyte with equal diffusivity $D_+=D_-=D$ and valence $z_+=z_-=z$ for the two ionic species, ignoring cross terms and concentration dependence in the mobility tensor. Moreover, we restrict our attention to the simplest prototypical microelectrochemical system, consisting of the electrolyte confined between two parallel planar blocking electrodes at $x=\pm L$, as sketched in Fig. 1. By symmetry, this rules out any effects of surface conduction [52,56] or ac electro-osmotic flow [9–11] and allows us to focus on the strongly nonlinear response due to the excessive accumulation of ions in the screening layers at the electrodes. In summary, the system is identical to that studied in Ref. [1] (PNP) and Ref. [54] (MPNP), except that we apply an ac voltage rather than a step dc voltage and study the periodic response after all tran-

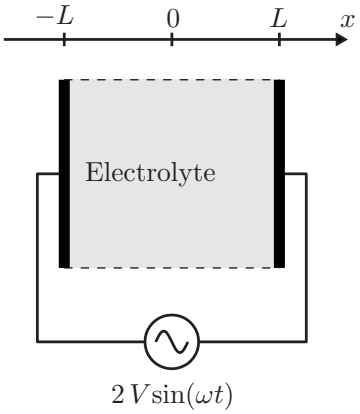

FIG. 1. Sketch of 1D model problem. The electrolyte is confined between parallel-plate blocking electrodes separated by a gap of width $2L$, and a harmonic potential of $V_{\mathrm{ext}}(t)=\pm V\sin(\omega t)$ is applied to the left and right electrodes, respectively, so the overall potential drop across the cell is $2V\sin(\omega t)$; this corresponds to a $4V$ peak-to-peak voltage or $\sqrt{2}V$ rms.

sients have decayed. We shall see that imposing an external time scale (the ac period) fundamentally alters the dynamics and complicates the analysis.

B. Dimensionless form in one dimension

We cast the problem into dimensionless form using L as the reference length scale and the RC relaxation time $\tau=\lambda_D L/D$ as the reference time scale [1], so that time and space are represented by the dimensionless variables $t'=t/\tau$ and $x'=x/L$. The potential and ionic concentrations are rescaled as $\phi'=\phi ze/kT$ and $c'_{\pm}=c_{\pm}/c^*$, where kT/e is the thermal voltage scale and c^* is the nominal bulk electrolyte concentration.

After dropping the primes from the dimensionless variables, the governing equations take the form

$$-\epsilon^2\partial_x^2\phi=\tfrac{1}{2}(c_+-c_-), \tag{9}$$

$$\partial_t c_{\pm}=-\epsilon\partial_x F_{\pm}, \tag{10}$$

where the fluxes $F_{\pm}$ are given by

$$F_{\pm}=-c_{\pm}\partial_x\mu_{\pm}. \tag{11}$$

For a dilute electrolyte the electrochemical potentials reduce to

$$\mu_{\pm}=\ln c_{\pm}\pm\phi, \tag{12}$$

and we arrive at the Nernst-Planck equations in dimensionless form,

$$\partial_t c_{\pm}=\epsilon\partial_x(\partial_x c_{\pm}\pm c_{\pm}\partial_x\phi). \tag{13}$$

When steric exclusion is taken into account we get

$$\mu_{\pm}=\ln c_{\pm}\pm\phi-\ln(1-\nu c), \tag{14}$$

where the parameter $\nu=2c^*a^3$ is the nominal volume fraction of the ions in the electrolyte [53].

It is convenient to introduce also the average ion or "salt" concentration and (half) the charge density

$$c=\tfrac{1}{2}(c_++c_-),\quad \rho=\tfrac{1}{2}(c_+-c_-), \tag{15}$$

in terms of which the transport equations can be rewritten as

$$\partial_t c=-\epsilon\partial_x F, \tag{16}$$

$$\partial_t\rho=-\epsilon\partial_x J. \tag{17}$$

Here, $F=\frac{1}{2}(F_++F_-)$ and $J=\frac{1}{2}(F_+-F_-)$ are the average salt flux and current density, respectively,

$$F=-\partial_x c/(1-\nu c)-\rho\partial_x\phi, \tag{18}$$

$$J=-\partial_x\rho-c\partial_x\phi-\nu\rho\partial_x c/(1-\nu c). \tag{19}$$

Since we assume blocking electrodes we have no-flux boundary condition at the electrodes,

$$F_{\pm}=0\quad\text{or}\quad F=J=0, \tag{20}$$

whereas the compact-layer boundary condition reduces to

$$V_{\mathrm{ext}}-\phi=\mp\epsilon\delta\partial_x\phi\quad\text{at } x=\pm 1. \tag{21}$$

Here, $V_{\mathrm{ext}}(t)=\mp V\sin(\omega t)$ is the electrode potential and $\delta=C_D/C_S$ is the ratio of the compact-layer capacitance $C_S=\varepsilon_S/h_S$ to that of the diffuse layer $C_D=\varepsilon/\lambda_D$ in the low-voltage limit.

C. Dimensionless parameters

The PNP model contains three dimensionless parameters: ϵ, V, and δ. In aqueous electrolytes, the screening length has submicron scale, $\lambda_D\approx 1-100$ nm, so the diffuse-charge boundary layers near the electrodes typically have a very small dimensionless width $\epsilon=\lambda_D/L\ll 1$, at least in microsystems where $L\gg 1$ μm. Although $\epsilon>1$ is possible in nanosystems, we restrict our attention to the typical case $\epsilon\ll 1$, which is the basis for our asymptotic analysis.

Contrary to most prior work, we focus on the nonlinear regime of large applied voltages, $V\gg 1$ (or, with units, $V\gg kT/e\approx 25$ mV), as in Refs. [1,45,48,52–54]. Since applied voltages larger than a few volts tend to trigger Faradaic reactions in aqueous electrolytes at ac frequencies around the inverse RC time [12,85], we envision experimentally relevant values of $V\approx 1-200$, although larger voltages can be sustained at higher frequencies or in nonaqueous solvents or liquid salts. Unlike prior work, we allow for large enough voltages that the double layers lose their quasiequilibrium structure.

The parameter $\delta=C_D/C_S=\lambda_S/\lambda_D$ (where $\lambda_S=h_S\varepsilon/\varepsilon_S$ is an effective thickness for the compact layer) can be estimated in some cases, but it is usually adjusted to fit experimental data. For example, let us consider different surfaces in contact with a 1 mM aqueous electrolyte with $\lambda_D=10$ nm. For a thin dielectric coating, such as a natural TiO_2 oxide layer with $h_S=4$ nm and $\varepsilon_S=110$ where a constant C_S seems reasonable, we get $\delta\approx 0.3$, although much thicker dielectric layers yielding $\delta\approx 10$ can arise in patterned microsystems [17]. In nonlinear electrokinetic phenomena, the inferred value of δ, required to match the standard dilute-solution model to experimental data, can be up to several orders of magnitude

larger, although this is more likely due to failures of the model, and not directly related to surface capacitance [58].

With a dielectric electrode coating, the surface capacitance is relatively clear, but in the classical picture of the Stern model [59], it is associated with a hypothetical flat monolayer of water molecules, which limit the approach of hydrated ions at the metal/electrolyte interface. In that case, one would expect $h_S \approx 0.1$ nm and, since alignment of water dipoles is assumed to reduce the permittivity in the Stern layer to $\varepsilon_S \approx 0.1\varepsilon$ [86,87], we estimate $\delta \approx 0.1$. The Stern picture, however, is complicated (at least) by electronic boundary layers in the metal [88], chemisorption from the solution [89], nanoscale surface roughness [90,91], and crowding effects absent in the PNP model of the diffuse layer, all of which can be misattributed to the Stern layer, as emphasized by Bazant *et al.* [58]. Even for a smooth liquid-mercury electrode, the inferred Stern layer capacitance is voltage dependent [86,89]. Nevertheless, since our goal here is to analyze the nonlinear dynamics of ions in solution, we will simply assume a constant surface capacitance and allow for a wide range of values $\delta = 0.01 - 10$.

In the simple MPNP model there is one more dimensionless parameter, $\nu = 2a^3 c^*$, which controls the importance of crowding effects. The nominal concentration c^* could range from a very dilute 1 μM solution with 6×10^{20} ions/m^3 to a concentrated 1 M solution (near physiological salt levels) with 6×10^{26} ions/m^3. A natural choice for the effective molecular lattice spacing a is the diameter of a hydrated ion, around 0.4–0.5 nm for small ions in water, which would yield $\nu \approx 10^{-7} - 10^{-1}$. Taking into account the underestimation of steric effects in a hard-sphere liquid by our lattice-based model [58,74], the value of a could be increased by roughly a factor of 2 [69]. Electrostatic correlations also become important when ions are crowded at this scale, comparable to the Bjerrum length of 0.7 nm in bulk water. As a crude approximation, therefore, we may consider ν as large as 0.4 in a concentrated electrolyte.

D. Numerical solution

Before embarking on our asymptotic analysis, we present some numerical solutions of the PNP model for the problem sketched in Fig. 1, which will be used to test and calibrate various analytical approximations below. As noted above, steric effects in the MPNP model tend to reduce nonlinearities, so the PNP model serves as a more stringent test case.

We use the COMSOL finite element package [92] to solve numerically the PNP model in the form of Eqs. (9), (16), and (17) with boundary conditions (20) and (21). It is necessary to use a very fine mesh of $\Delta x_{\min} \approx 10^{-5}$ close to the electrodes in order to resolve the highly compressed (and unphysical) diffuse-layer structure in the PNP model, even at $\epsilon = 10^{-3}$. For our 1D problem, this is straightforward to achieve using a nonuniform graded mesh, but in two or three dimensions it would pose a serious problem. In fact, overcoming such limitations is a major motivation for our development of accurate boundary-layer approximations below. The steady-state periodic response is obtained by integrating forward in time, using the default time-dependent solver of COMSOL. Since the transient diffusive relaxation in the bulk is slow, it is necessary to integrate for a very long time, up to 100 times the period of the driving voltage or more, before the steady-state periodic solution is reached.

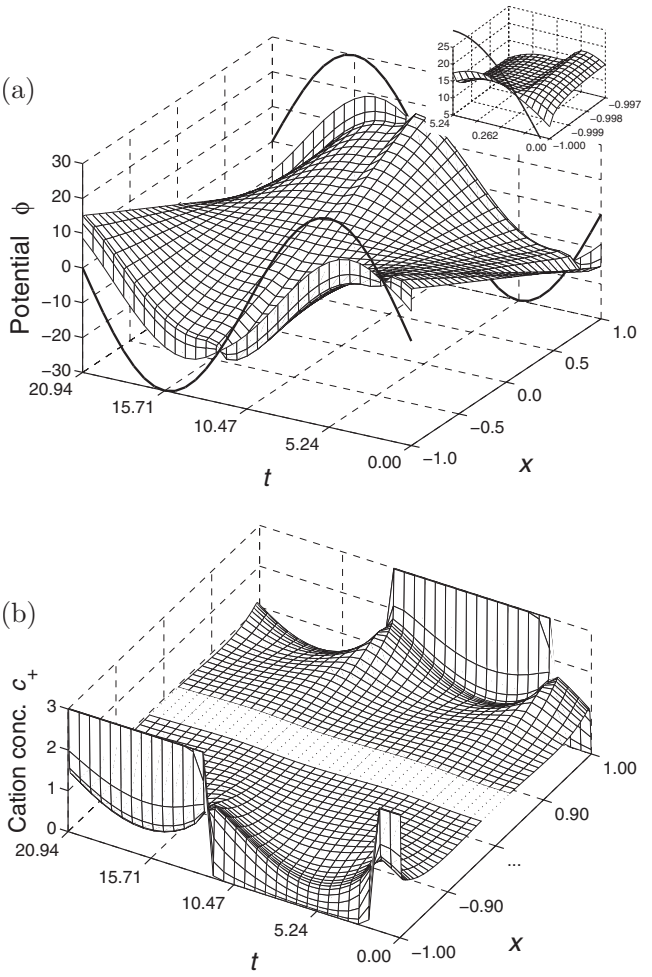

FIG. 2. Numerical solution of the PNP equations for $V=30$, $\omega=0.3$, $\delta=0.3$, and $\epsilon=0.001$. (a) Potential variation in time and space; solid black line shows the external potential on the electrodes V_{ext}. The inset zooms onto the rapid potential variation across the diffuse screening layer. (b) Zoom on cation concentration near the electrodes; anion concentration is identical but phase shifted one half period in time.

Figure 2 shows the result for $V=30$, $\omega=0.3$, $\delta=0.3$, and $\epsilon=0.001$: Fig. 2(a) shows the potential $\phi(x,t)$, and Fig. 2(b) displays the cation concentration profile $c_+(x,t)$. In the bulk region both the cation and anion concentrations are constant and (very close to) unity, and the electrolyte therefore behaves like an ideal resistive medium with unit conductivity. The potential varies linearly throughout the bulk region, driving a constant Ohmic current density, and shows a roughly harmonic time variation that is about 45° ahead of the electrode potential $V_{\text{ext}} = \mp V \sin(\omega t)$ (solid black line at $x = \pm 1$).

In the diffuse screening layer close to the electrodes the ion concentration varies very rapidly from a maximum of $\max\{c_\pm\} \approx 3 \times 10^3$ at the electrode surface down to around unity over a distance of $O(\epsilon)$. The inset in Fig. 2(a) zooms

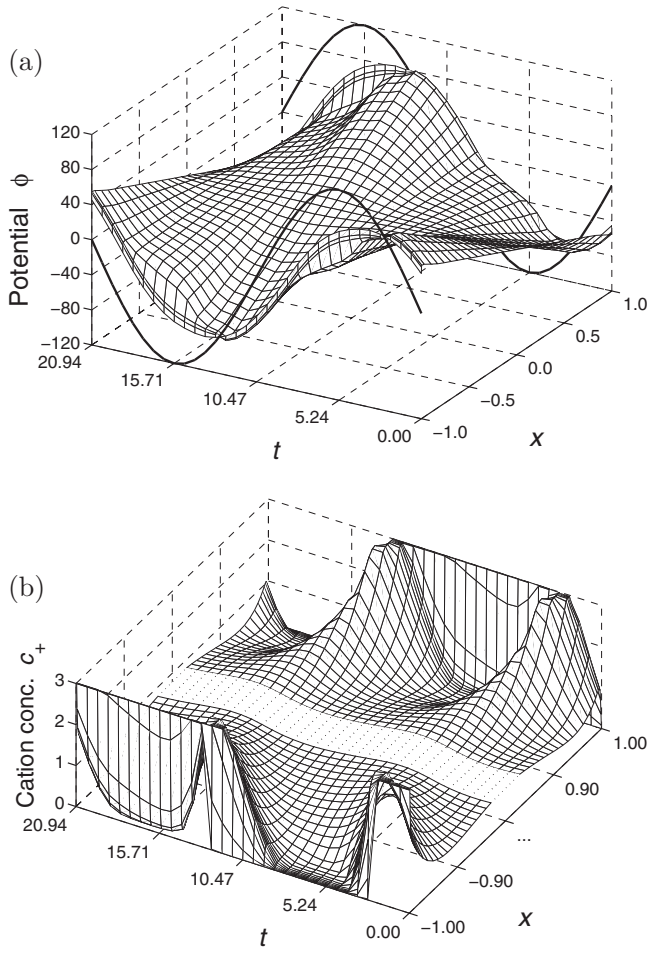

FIG. 3. Numerical solution of the PNP equations for $V=120$, $\omega=0.3$, $\delta=0.3$, and $\epsilon=0.001$. (a) Potential variation in time and space. (b) Zoom on cation concentration near the electrodes.

onto the rapid potential variation in the screening layer, and the visible difference between the potentials on the electrode and in the electrolyte corresponds to the compact-layer voltage [cf. Eq. (21)].

Within a distance of about 0.1 from the electrodes we see a nonuniform pattern in the cation concentration profile that oscillates at twice the driving frequency. The concentration has a minimum just about the time when the screening layer is fully charged and a maximum when the screening layer changes polarity (occurs for $t\approx 1.75$ and again at 12.25). The anion concentration shows a fully similar pattern, so that effectively this "diffusion layer" is charge neutral.

Figure 3 shows the solution for $V=120$ with otherwise the same parameters as in Fig. 2. The overall picture is essentially the same as before: the bulk ionic concentrations are constant, but due to the massive accumulation of ions around the electrodes (maximal concentration exceeds 4×10^4) the bulk concentration is down to 0.86, i.e., 14% below the nominal value.

An interesting feature is seen in Fig. 3(b) for $t\approx 5.24$: close to the electrode at $x=-1$ there is an extended region where the cation concentration drops to zero, while at the same time the anion concentration is also low but clearly nonzero (see Fig. 14 below for a more detailed view). This transient "space-charge layer" is similar to the steady counterpart described by Rubinstein and Shtilman for the case of dc Faradaic conduction when an electrochemical cell is driven above the diffusion-limited current [47,48]. It is also clear from Fig. 3(a) that there is a significant potential drop across the space-charge layer.

III. ASYMPTOTIC ANALYSIS

A. Nested boundary layers

In the limit of thin double layers, $\epsilon=\lambda_D/L\ll 1$, the dynamical problem can be analyzed by matched asymptotic expansions [1]. The standard procedure begins by seeking regular expansions in the form of power series

$$c = c^{(0)} + \epsilon c^{(1)} + \epsilon^2 c^{(2)} + \cdots, \tag{22}$$

substituting into the governing equations, and collecting like powers of ϵ. This procedure is guaranteed to converge in the limit $\epsilon\to 0$ with all other parameters held fixed. However, for any fixed $\epsilon>0$ there could be ϵ-dependent restrictions on the other parameters, in particular the driving voltage V, for a truncated expansion to produce accurate results. Following Bazant and co-workers [1,52] we denote the regime where such conditions hold as "weakly nonlinear," as opposed to the "strongly nonlinear" regime where the standard asymptotic expansions breaks down. It is on this strongly nonlinear regime that we focus our attention. We aim at deriving the leading-order dominant balance in the joint limit $\epsilon\to 0$ and $V\to\infty$, and since we focus exclusively on the leading-order approximation, we drop the superscript $^{(0)}$ on all variables in order to simplify the notation.

For small applied voltages, it is well known that in the limit $\epsilon\to 0$ the diffuse part of the double layer acts as a mathematical boundary layer of $O(1)$ nonzero charge density and $O(\epsilon)$ thickness on the leading-order quasielectroneutral bulk region at the $O(1)$ length scale of the geometry. This is the mathematical justification for linear circuit models. In the case of blocking electrodes, the characteristic RC time scale for charging of the double layers is $O(1)$ in our dimensionless units.

The application of a large voltage leads to the new effect of salt adsorption by the diffuse layer and related depletion of the bulk concentration, first described by Bazant *et al.* [1], and in higher dimensions, surface conduction through the diffuse layer becomes important at the same time [52]. For a suddenly applied dc voltage at blocking electrodes, during the initial RC charging phase over $O(1)$ time, a thin quasielectroneutral diffusion layer extends to $O(\sqrt{\epsilon})$ width. The next phase of relaxation proceeds at the slow $O(\epsilon^{-1})$ time scale for bulk diffusion, as concentration gradients spread across the cell to $O(1)$ distances.

For a large applied ac voltage, this picture is altered by the imposed time scale. In the case of ac forcing close the RC time scale, $\omega^{-1}=O(1)$, the oscillating voltage generally leads to the formation of a thin nested *oscillating diffusion layer* confined to steady $O(\sqrt{\epsilon})$ thickness. Since salt adsorption by the inner diffuse layer is positive, regardless of the polarity, the diffusion layer oscillates at twice the driving

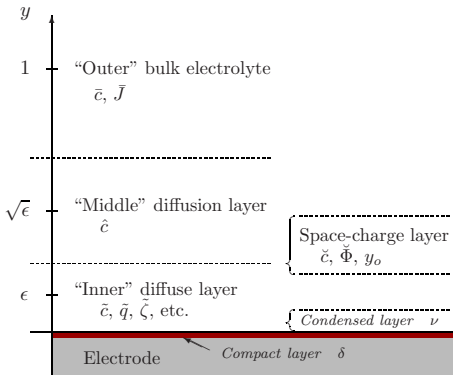

FIG. 4. (Color online) Schematic picture of nested boundary layers in matched asymptotic expansion: the bulk outer region is connected via the middle diffusion layer to the inner diffuse layer. A compact (Stern) layer separates the electrolyte from the blocking electrode. At large voltage, local salt depletion in the diffusion layer can cause the double layer to change to a nonequilibrium structure, with an extended "space-charge" layer that is completely depleted of coions. Further, when the concentration in the diffuse layer approaches the steric limit, a condensed phase of ions forms at the electrode. The figure also indicates some of the variables and parameters introduced in the asymptotic analysis of the different layers.

frequency. It is also accompanied by a gradual bulk salt depletion that propagates across the cell over $O(1)$ times after the ac voltage is turned on, similar to the case of the sudden dc voltage. However, in this work, we ignore such initial transients and focus on the steady ac response after the bulk has relaxed to steady state.

In this way, we are lead to analyze the nested boundary-layer structure sketched in Fig. 4, consisting of the "outer" bulk region (unit length scale), a "middle" diffusion layer ($\sqrt{\epsilon}$ length scale), and the "inner" diffuse part of the double layer (ϵ length scale). This picture remains valid until the voltage becomes large enough to fully deplete the middle diffusion layer, leading to the formation of transient space-charge layers extending by $O(\sqrt{\epsilon})$ or more into the cell, twice per ac period. Our goal in the rest of the paper is to develop uniformly valid asymptotic boundary-layer approximations in all of these cases. For clarity, we denote asymptotic approximations for each region by different accents, as indicated in Fig. 4. For example, the salt concentration c is asymptotic to $\bar{c}$ in the bulk, $\hat{c}$ in the diffusion layer, $\tilde{c}$ in the diffuse-charge layer, and $\check{c}$ in the space-charge layer.

B. Quasielectroneutral bulk

We begin by analyzing the solution in the bulk region. The Poisson equation (9) shows that the charge density vanishes to both zeroth and first orders in ϵ, so that at leading order

$$\bar{c}_+ = \bar{c}_- = \bar{c}, \tag{23}$$

denoting bulk variables by an overbar accent. The bulk salt concentration displays diffusive dynamics on the time scale $\bar{t}=\epsilon t$ [1], but on the *RC* time scale the concentration profile is constant in time $\bar{c}=\bar{c}(x)$. Here, we focus on the steady state after the bulk transients have relaxed, and by symmetry of our simple model problem the bulk concentration is then simply constant in space, $\bar{c}=\bar{c}_o$. The leading-order potential varies linearly in space,

$$\bar{\phi} = -\frac{\bar{J}(t)}{\bar{c}_o}x, \tag{24}$$

where $\bar{J}(t)$ is the Ohmic current and $\bar{c}_o$ acts as the bulk conductivity.

In the weakly nonlinear regime the bulk concentration is at the nominal value, $\bar{c}_o=1$, whereas in the strongly nonlinear regime the adsorption of ions in the double layers may be so strong as to induce $\bar{c}_o<1$. The problem has the following symmetries about the origin:

$$\phi(x,t) = -\phi(-x,t),$$

$$\rho(x,t) = -\rho(-x,t),$$

$$c(x,t) = c(-x,t). \tag{25}$$

In Secs. III C–III E below we focus on the nested boundary layers developing at the *left* electrode, and for convenience we therefore perform a change of variables, $y=1+x$, such that $y=0$ corresponds to the electrode surface and $y>0$ corresponds to the interior of the cell.

C. Quasiequilibrium double layer

The singular perturbation in the Poisson equation (9) gives rise to a boundary layer of width $O(\epsilon)$ where the charge density is nonzero to zeroth order in ϵ. Introducing a scaled spatial variable $\tilde{y}=y/\epsilon$ to remove the singular perturbation, we can seek regular asymptotic expansions (denoted by overtilde accents) in the inner diffuse layer. Substituting into Eqs. (10) and (11) and using $\partial_{\tilde{y}}=\epsilon\partial_y$, we find that the double layer is in quasiequilibrium at leading order with constant electrochemical potential $\tilde{\mu}_\pm$ across it. The value of $\tilde{\mu}_\pm$ is determined by matching with the solution in the adjacent quasielectroneutral diffusion layer,

$$\tilde{\mu}_\pm = \lim_{\hat{y}\to 0}\{\ln \hat{c} \pm \hat{\phi}\}. \tag{26}$$

The quasiequilibrium arises because the diffuse-charge distribution relaxes on the Debye time scale $\tilde{t}=t/\epsilon$, which is much faster than the *RC* charging time. The ion distributions are determined from Eq. (14) as

$$\tilde{c}_\pm = \frac{\hat{c}_s e^{\mp\tilde{\psi}}}{1+\nu\hat{c}_s(\cosh\tilde{\psi}-1)}, \tag{27}$$

where $\tilde{\psi}=\tilde{\phi}-\hat{\phi}$ is the excess potential in the double layer relative to the diffusion layer, and $\hat{c}_s$ is the limiting value of the salt concentration $\hat{c}_s=\lim_{y\to 0}\hat{c}$. The excess potential satisfies the MPB equation

$$\partial_{\tilde{y}}^2\tilde{\psi} = \frac{\hat{c}_s \sinh\tilde{\psi}}{1 + \nu\hat{c}_s(\cosh\tilde{\psi} - 1)}, \tag{28}$$

which can be integrated once to get the field [53,68]

$$\partial_{\tilde{y}}\tilde{\psi} = -\operatorname{sgn}(\tilde{\psi})\sqrt{2\ln[1 + 2\nu\hat{c}_s \sinh^2(\tilde{\psi}/2)]/\nu}. \tag{29}$$

Note that the ion concentrations in Eq. (27) are bounded above by steric exclusion, $\tilde{c}_\pm \leq 2/\nu$, while at much lower concentrations they reduce to the usual results from dilute theory: in this limit ($\nu \to 0$) the ion profiles are given by the Boltzmann equilibrium distribution,

$$\tilde{c}_\pm = \hat{c}_s e^{\mp\tilde{\psi}}, \tag{30}$$

and we obtain the standard PB equation

$$\partial_{\tilde{y}}^2\tilde{\psi} = \hat{c}_s \sinh\tilde{\psi}, \tag{31}$$

yielding the familiar Gouy-Chapman (GC) solution

$$\tilde{\psi} = 4\tanh^{-1}[\tanh(\tilde{\zeta}/4)e^{-\sqrt{\hat{c}_s}\tilde{y}}]. \tag{32}$$

Here, the integration constant $\tilde{\zeta} = \tilde{\psi}(0)$ is simply the leading-order zeta potential, and $1/\sqrt{\hat{c}_s}$ is the local effective Debye length.

Variations of the ion mobility with concentration could lead to somewhat slower relaxation in the highly crowded double layer. However, the quasiequilibrium ion distribution is independent of our simplifying assumptions regarding equal ion mobility, neglect of cross terms, and concentration dependence.

D. Surface conservation laws

The redistribution of ions across the diffuse layer is instantaneous on the *RC* time scale, but the total amount of ions adsorbed can change only by flux into the layer from the adjacent diffusion layer. Following Bazant and co-workers [1,52–54,56] we quantify this by considering the excess amount of each ionic species accumulated in the double layer, $w_\pm = \epsilon\tilde{w}_\pm$, where

$$\tilde{w}_\pm = \frac{1}{\epsilon}\int_{\text{d.l.}} (\tilde{c}_\pm - \hat{c}_\pm)dy = \int_0^\infty (\tilde{c}_\pm - \hat{c}_\pm)d\tilde{y}. \tag{33}$$

The time evolution of $\tilde{w}_\pm$ is then determined by

$$\partial_t\tilde{w}_\pm = \int_0^\infty \partial_t(\tilde{c}_\pm - \hat{c}_\pm)d\tilde{y} = -\lim_{\tilde{y}\to\infty}\tilde{F}_\pm \tag{34}$$

$$= -\lim_{\hat{y}\to 0}\hat{F}_\pm, \tag{35}$$

where the last equality is obtained by flux matching between the double layer and diffusion layer. We also define the diffuse charge and surface excess salt by

$$\tilde{q} = \tfrac{1}{2}(\tilde{w}_+ - \tilde{w}_-), \quad \tilde{w} = \tfrac{1}{2}(\tilde{w}_+ + \tilde{w}_-). \tag{36}$$

Since the diffusion layer is quasielectroneutral at leading order, the double-layer charging process is coupled directly to the bulk electric current

$$\partial_t\tilde{q} = -\bar{J}(t). \tag{37}$$

Variations in the excess salt $\tilde{w}$ are coupled to the dynamics in the diffusion layer

$$\partial_t\tilde{w} = -\lim_{\hat{y}\to 0}\hat{F} \equiv -\tilde{F}_o, \tag{38}$$

where the flux injection $\tilde{F}_o(t)$ at the inner "edge" of the diffusion layer should be understood as the *driving force* behind the oscillations in the salt concentration in the diffusion layer. These relations exemplify the general mathematical theory of surface conservation laws, in which the total excess concentrations in a diffuse interface are coupled to normal (and surface) fluxes in a concentrated solution [56].

E. Oscillating diffusion layer

The diffuse screening layers at the electrodes periodically adsorb and expel an excess amount of ions from the surrounding electrolyte. However, the bulk transport of neutral salt is essentially a diffusion process on the time scale $\bar{t} = \epsilon t$, which is much slower than the ac driving that we consider here, and hence the leading-order dynamics are confined to a diffusion layer of $O(\sqrt{\epsilon})$ width around the electrode [1,52]. We therefore introduce a scaled spatial variable $\hat{y} = y/\sqrt{\epsilon}$ and seek regular asymptotic expansions (denoted by hat accents) in this middle diffusion layer. Substituting into the Poisson equation (9) we find that, like in the bulk, the charge density vanishes to zeroth order in ϵ, so that the leading-order ion concentrations are equal,

$$\hat{c}_+ = \hat{c}_- = \hat{c}. \tag{39}$$

Equation (16) then reduces to a simple diffusion problem,

$$\partial_t\hat{c} = \partial_{\hat{y}}^2\hat{c}, \tag{40}$$

to be solved on the interval $\hat{y} \in [0,\infty)$. Matching to the bulk solution requires $\lim_{\hat{y}\to\infty}\hat{c} = \lim_{y\to 0}\bar{c} = \bar{c}_o$, whereas the boundary condition at the inner edge of the diffusion layer is determined by matching with the salt flux out of the double layer [cf. Eq. (38)]

$$-\frac{1}{\sqrt{\epsilon}}\lim_{\hat{y}\to 0}\partial_{\hat{y}}\hat{c} = \lim_{\hat{y}\to 0}\hat{F} = \tilde{F}_o. \tag{41}$$

The solution to the 1D diffusion problem can be expressed in terms of a convolution integral,

$$\hat{c} = \bar{c}_o + \sqrt{\epsilon}\int_{-\infty}^{t} G(\hat{y}, t - t')\tilde{F}_o(t')dt', \tag{42}$$

where

$$G(\hat{y},t) = \frac{1}{\sqrt{\pi t}}e^{-\hat{y}^2/4t} \tag{43}$$

is the Green's function for the diffusion equation with a sudden unit flux at $t = 0^+$ injected at the boundary,

$$G(\hat{y},0) = 0, \quad -\partial_{\hat{y}}G(0^+,t) = \delta^+(t), \tag{44}$$

for a semi-infinite domain. Technically, Eq. (43) is the first term in an expansion for the Green's function in a finite bulk

domain (Eq. (24) of Ref. [1]), which would be needed to describe the initial transient when the ac voltage is first turned on. Here, we focus on the steady-state response, after initial diffusion layers have relaxed across the cell, thereby lowering the uniform bulk concentration $\bar{c}$ (see below), and the oscillating diffusion layers have only $O(\sqrt{\epsilon})$ width, consistent with the semi-infinite approximation (43).

To describe this situation, since the flux injection is periodic we may rewrite Eq. (42) as

$$\hat{c} = \bar{c}_o + \sqrt{\epsilon}\int_0^T G_\omega(\hat{y}, t-t')\tilde{F}_o(t')dt', \tag{45}$$

where $T=2\pi/\omega$ is the driving period and

$$G_\omega(\hat{y},t) = \frac{1}{T}\left[-\hat{y} + \sum_{n=1}^{\infty}\frac{1}{\sqrt{in\omega}}e^{in\omega t-\sqrt{in\omega}\hat{y}} + \text{c.c.}\right] \tag{46}$$

is the Green's function for a periodic influx of salt,

$$\langle G_\omega(0,t)\rangle = 0, \quad -\partial_{\hat{y}}G_\omega(0^+,t) = \sum_{n=-\infty}^{\infty}\delta^+(t-nT). \tag{47}$$

Equation (42) or Eq. (45) clearly shows that in the weakly nonlinear regime, where $\tilde{F}_o$ is $O(1)$, the concentration $\hat{c}$ in the diffusion layer is equal to the bulk $\bar{c}$ at leading order; the flux injection only gives rise to an $O(\sqrt{\epsilon})$ perturbation. The strongly nonlinear regime is essentially *defined* as the regime of driving voltages high enough that $\tilde{w}$ and $\tilde{F}_o$ grow to $O(1/\sqrt{\epsilon})$ and the variations in $\hat{c}$ reach $O(1)$.

Since the diffusion layer is charge neutral at leading order, the current density is constant across it and equal to the bulk current $\bar{J}(t)$. However, the conductivity differs from its bulk value, which gives rise to *transient concentration polarization*. There is an excess electrostatic potential variation $\hat{\psi} = \hat{\phi} - \bar{\phi}$, and an excess field given by

$$-\frac{1}{\sqrt{\epsilon}}\partial_{\hat{y}}\hat{\psi} = \bar{J}\left(\frac{1}{\hat{c}} - \frac{1}{\bar{c}}\right), \tag{48}$$

that can be integrated to

$$\hat{\psi}(\hat{y}) = \sqrt{\epsilon}\bar{J}\int_{\hat{y}}^{\infty}\left(\frac{1}{\hat{c}} - \frac{1}{\bar{c}}\right)d\hat{y}. \tag{49}$$

In the weakly nonlinear regime we can expand $1/\hat{c}$ as $1/\hat{c} \approx 1/\bar{c} - (\hat{c}-\bar{c})/\bar{c}^2 + O(\epsilon)$ to get $\hat{\psi}(0) = \epsilon\bar{J}(\tilde{w} - \langle\tilde{w}\rangle)$ at leading order; in the strongly nonlinear regime $\hat{\psi}$ grows to $O(\sqrt{\epsilon/\omega}\bar{J})$ which is, however, still negligible compared to the bulk potential $\bar{\phi} = -\bar{J}x/\bar{c}_o$.

Finally, the leading-order charge density in the diffusion layer can be evaluated by substituting Eq. (48) into the Poisson equation to get

$$\hat{\rho} = -\epsilon\partial_{\hat{y}}^2\hat{\psi} = -\epsilon^{3/2}\frac{\bar{J}\partial_{\hat{y}}\hat{c}}{\hat{c}^2}. \tag{50}$$

The quasielectroneutral solution in the diffusion layer remains valid for $|\hat{\rho}| \ll \hat{c}$; we return to this aspect in Sec. VI.

F. Closing the problem

In order to close the coupled problem for the dynamical variables $\bar{J}(t)$, $\tilde{q}(t)$, $\tilde{\zeta}(t)$, $\tilde{w}(t)$, and $\hat{c}_s(t)$ we need a few more relations between them. The first is obtained by writing the overall potential drop over the boundary layers, from the electrode to the bulk electrolyte at $x=-1$, as the sum of the contributions from the compact and diffuse layers

$$V_{\text{ext}} - \bar{\phi}(-1,t) = V_{\text{ext}} - \bar{J}/\bar{c}_o = -\tilde{q}\delta + \tilde{\zeta}. \tag{51}$$

Since we focus on the leading-order approximation, we neglect here the small potential drop over the diffusion layer. Next, the diffuse-layer voltage $\tilde{\zeta}$ can be related to the diffuse charge through Eq. (29) for the field at the electrode surface, yielding Freise's formula [68]

$$\tilde{q} = -\text{sgn}(\tilde{\zeta})\sqrt{2\ln[1+2\nu\hat{c}_s\sinh^2(\tilde{\zeta}/2)]/\nu}, \tag{52}$$

and in the dilute limit this reduces to Chapman's formula

$$\tilde{q} = -2\sqrt{\hat{c}_s}\sinh(\tilde{\zeta}/2). \tag{53}$$

The charge-voltage relation can be inverted to get

$$\tilde{\zeta} = -\text{sgn}(\tilde{q})2\sinh^{-1}\sqrt{\frac{e^{\nu\tilde{q}^2/2}-1}{2\nu\hat{c}_s}}. \tag{54}$$

The excess salt concentration can be expressed in integral form [54]

$$\tilde{w} = \int_0^{\tilde{\zeta}}\frac{\tilde{c}}{\partial_{\tilde{y}}\tilde{\psi}}d\tilde{\psi}, \tag{55}$$

and using PB theory in the dilute limit the integral can be evaluated to [1]

$$\tilde{w} = 4\sqrt{\hat{c}_s}\sinh^2(\tilde{\zeta}/4), \tag{56}$$

or eliminating $\tilde{\zeta}$ we obtain

$$\tilde{w} = \sqrt{\tilde{q}^2 + 4\hat{c}_s} - \sqrt{4\hat{c}_s}. \tag{57}$$

For the MPB model, Eq. (55) is difficult to handle analytically, but numerical integration shows that Eq. (57) approximates the integral well, with a relative error of $O(\nu)$.

The bulk salt concentration $\bar{c}_o$ is determined by imposing the global conservation of salt in the cell,

$$\int_{-1}^{1} c(x,t)dx = 2. \tag{58}$$

As noted in Ref. [45], integral constraints on the total number of inactive ions are generally required for steady-state problems to replace information about the initial condition (e.g., when the voltage is first turned on) that is preserved during time evolution with no-flux boundary conditions.

There is a periodic exchange of salt between the inner diffuse and middle diffusion layers, but Eq. (45) shows that $\langle\hat{c}\rangle = \bar{c}$, i.e., the diffusion layer does not contain any *excess* salt on time average. As a result, the uniform bulk concentration in the (time-periodic) steady state, $\bar{c}_o$, is reduced only by the time-averaged salt adsorption of the diffuse layers,

$$\bar{c}_o = 1 - \epsilon\langle\tilde{w}\rangle, \tag{59}$$

which also describes the (static) steady state after a sudden dc voltage is imposed [1]. This, together with Eqs. (37), (38), (45), (51), (54), and (57), constitutes a set of "ordinary" (i.e., no partial) integro-differential-algebraic equations in time for the dynamical variables $\bar{J}(t)$, $\tilde{q}(t)$, $\tilde{F}_o(t)$, $\tilde{w}(t)$, $\hat{c}_s(t)$, and $\tilde{\zeta}(t)$.

Our focus in the present work is on the steady-state periodic response, and we explicitly made use of this in deriving our dynamical model by replacing the transient Eq. (43) with Eq. (46). The problem could be solved numerically by a relaxation method, representing each dynamical variable by a truncated Fourier series, as done in Ref. [75]. Here, however, our approach is to integrate the dynamical equations by a time-stepping algorithm; the integration is continued until a periodic state is reached, typically within 10–20 periods of the driving voltage. The time-stepping approach is well suited for integrating also the nonequilibrium model developed in Sec. VI and is much more efficient on computer memory for solving problems with two- or three-dimensional electrode geometry. Further details are given in our supplementary material [93].

IV. WEAKLY NONLINEAR REGIME

The weakly nonlinear regime defined in Ref. [1] is characterized by fluctuations in the diffusion layer salt concentration being only a small perturbation to the bulk value, so that $\hat{c}=\bar{c}=1$ at leading order. This is the response predicted by matched asymptotic expansions in the singular limit $\epsilon \to 0$ with all other parameters held fixed, including V. As such the dimensionless, leading-order response is *independent* of ϵ. We begin with an analysis of this regime, and the findings here form the basis for understanding the peculiarities of the strongly nonlinear regime in subsequent sections, where the solution has a nontrivial dependence on V and ϵ.

A. Charge-voltage relation

The only nonlinearity in the weakly nonlinear model arises from the diffuse-layer charge-voltage relation [Eq. (52)]. In Fig. 5 we plot the accumulated charge $\tilde{q}$ as a function of the overall potential drop $\tilde{\Psi}=\tilde{\zeta}-\tilde{q}\delta$ across the double layer for different values of the capacitance ratio δ and nominal ion volume fraction ν.

In the Debye-Hückel limit, $|\tilde{\zeta}| \ll 1$, Eq. (52) can be linearized to get simply $\tilde{q}=-\tilde{\zeta}=-\tilde{\Psi}/(1+\delta)$. At larger voltage the classical PB theory predicts a dramatic increase in the diffuse-layer capacitance, and $\tilde{q}$ grows exponentially with $\tilde{\zeta}$. In Fig. 5 this behavior shows directly on the curve $\delta=\nu=0$ (GC model) that bends up sharply for $\tilde{\Psi} \gtrsim 10$; at $\tilde{\Psi}=20$ the concentration in the diffuse layer [cf. Eq. (30)] exceeds 10^8 times the bulk concentration, which is absurdly high for aqueous electrolytes.

This well-known unphysical artifact of PB theory is alleviated (but not eliminated) in the Gouy-Chapman-Stern (GCS) model by assuming a finite compact-layer capacitance, corresponding to a positive value of δ. Then at large

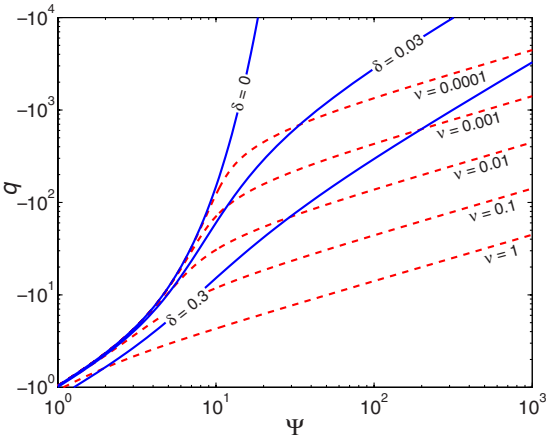

FIG. 5. (Color online) Quasisteady (dimensionless) accumulated charge $\tilde{q}$ in the double layer as a function of its voltage drop $\tilde{\Psi}=\tilde{\zeta}-\tilde{q}\delta$, plotted for different values of the Stern parameter δ with $\nu=0$ (solid line), and different values of the steric parameter ν with $\delta=0$ (dashed line), all in the weakly nonlinear regime with $\hat{c}=1$.

voltage the major part is carried by the compact layer, $\tilde{\Psi} \approx -\tilde{q}\delta$, while the diffuse-layer voltage remains small, $|\tilde{\zeta}| \approx 2\ln|\tilde{q}| \approx 2\ln|\tilde{\Psi}/\delta|$. This regularizes the problem at moderate voltages, but the success may be misleading: it is unlikely that a subnanometer-thick molecular Stern layer could withstand several volts without dielectric breakdown. Moreover, the GCS model does not impose a maximum charge density and at sufficiently large voltages still reaches unphysical ion concentrations.

A more realistic approach could account for crowding effects at large voltages using MPB theory [53,58], e.g., leading to the Bikerman-Freise (BF) model described above [60]. This is equivalent to PB theory at concentrations well below the steric limit, $\tilde{c}_\pm \ll 2/\nu$, as seen clearly in Fig. 5. However, once steric effects saturate the charge density, the diffuse-layer capacitance drops due to the condensed phase of ions forming at the electrode [53,58,59,68]. This occurs for $|\tilde{q}| \gtrsim \sqrt{2/\nu}$, and at still larger voltage the overall potential drop is primarily on the condensed layer, with Eq. (52) reducing to

$$|\tilde{q}| \approx \sqrt{\frac{2|\tilde{\zeta}|}{\nu}} \approx \sqrt{\frac{2|\tilde{\Psi}|}{\nu}}, \quad \text{for } |\tilde{\zeta}| \gg \ln(2/\nu). \tag{60}$$

Comparing the GCS model for a Stern monolayer with $\delta=0.03$ to the BF model, the latter predicts (much) lower charging already for $\tilde{\Psi} \gtrsim 30$ (or 750 mV) at $\nu=10^{-4}$. Even for our example of an oxide layer on the electrodes with $\delta=0.3$, crowding effects in the liquid could significantly affect the charge-voltage response for $\tilde{\Psi} \gtrsim 100$ (or 2.5 V), which is still within the range of many experiments.

This asymptotic square-root dependence of the charge-voltage relation (60) is a generic consequence of volume constraints [58], not only in Bikerman's lattice-gas model, but also in hard-sphere liquid models since it corresponds to a diffuse layer of uniform charge density. Once the con-

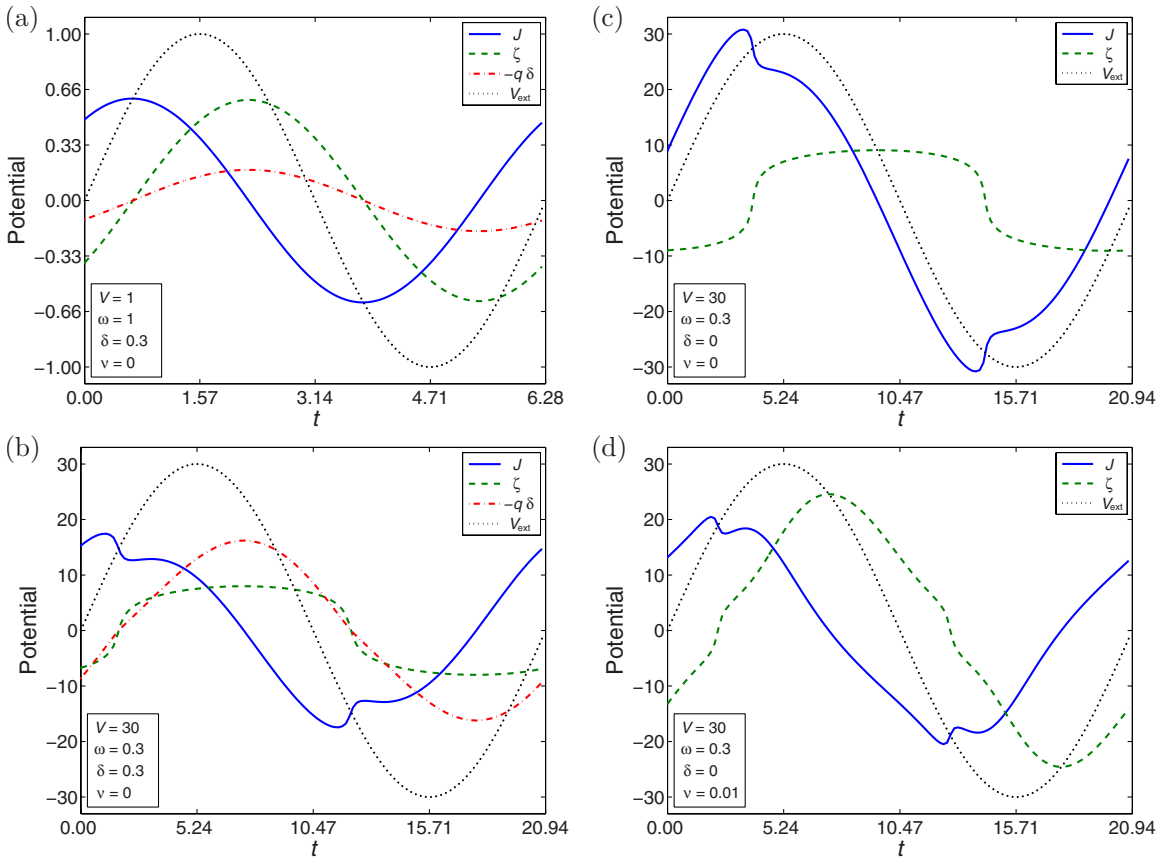

FIG. 6. (Color online) Distribution of dimensionless cell voltage, $V_{\rm ext}=\bar{J}+\tilde{\zeta}-\tilde{q}\delta$ (dotted line), divided into contributions across the bulk electrolyte $\bar{J}$ (solid line), diffuse layer ζ (dashed line), and compact layer $-q\delta$ (dashed-dotted line), all scaled to the thermal voltage kT/ze, as a function of time for different values of the parameters V, ω, δ, and ν. The panels show (a) Debye-Hückel limit, (b) Gouy-Chapman-Stern (GCS) model, (c) Gouy-Chapman (GC) model, and (d) Bikerman-Freise (BF) model.

densed layer forms, its voltage, $\approx\nu\tilde{q}^2/2$, can easily exceed that of the outer (PB) part of the diffuse layer, $\approx\ln(2/\nu)$, even while the latter remains thicker. The thickness of the condensed layer can be estimated to $\tilde{\ell}=\ell/\epsilon\approx\nu(|\tilde{q}|-\sqrt{2/\nu})$ [53], which remains a small fraction of the total diffuse-layer thickness until $|\tilde{q}|\gtrsim 1/\nu$.

Again we must emphasize that, strictly, imposing a maximum concentration of $2/\nu$ can be justified only *on average* over length scales larger than the (dimensionless) ion diameter a, whereas *pointwise* the concentration may well exceed $2/\nu$. For $\tilde{\ell}<\tilde{a}=a/\epsilon$, when the "condensed layer" is less that one ion diameter thick, it may therefore be more appropriate to employ the GCS model with $\delta\approx 1/\tilde{a}$ to model the closest approach of the very first monolayer of ions to the electrode surface. Nevertheless, since our focus in the present paper is on the dynamic response at large applied voltages, we will disregard any layering within the condensed layer, and use Bikerman's simple and analytically tractable model to account qualitatively for the impact of volume constraints on the system dynamics.

B. Dynamical response

The leading-order dynamic response in the weakly nonlinear regime is governed by

$$\partial_t\tilde{q}=-\bar{J}, \tag{61}$$

$$V_{\rm ext}=\bar{J}+\tilde{\zeta}-\tilde{q}\delta, \tag{62}$$

$$\tilde{\zeta}=2\,\sinh^{-1}\sqrt{\frac{e^{\nu\tilde{q}^2/2}-1}{2\nu}}, \tag{63}$$

$$\hat{c}=\bar{c}=1. \tag{64}$$

This may be rewritten as a single ordinary differential equation for the double-layer voltage $\tilde{\Psi}$ [1],

$$C\partial_t\tilde{\Psi}=\bar{J}=V_{\rm ext}-\tilde{\Psi}, \tag{65}$$

where $C(\tilde{\Psi})=-d\tilde{q}/d\tilde{\Psi}$ is the total differential capacitance of the double layer and $V_{\rm ext}(t)=V\sin(\omega t)$ is the external driving voltage.

We focus on the periodic response obtained by starting from an initially uncharged state and integrating forward in time until all transients have died out. Figure 6 shows the results for different values of the model parameters.

Figure 6(a) shows the result for $V=1$, $\omega=1$, $\delta=0.3$, and $\nu=0$. At this low voltage the charge-voltage relation is still essentially linear, so the system behaves like a linear *RC*

circuit with time constant $(1+\delta)^{-1}$. The double-layer voltage $\tilde{\Psi}$ is dominated by the diffuse layer with the compact layer contributing only a small fraction δ.

Figure 6(b) shows the solution at larger voltage $V=30$ with $\omega=0.3$, $\delta=0.3$, and $\nu=0$. At this voltage the relation between $\tilde{\zeta}$ and $\tilde{q}$ is clearly nonlinear, $\tilde{\zeta}$ stalls for $|\tilde{q}| \gtrsim 10$, and the double-layer voltage becomes dominated by the compact layer. When the double layer changes polarity this in turns makes the change of sign of $\tilde{\zeta}$ look like a "sharp" transition which gives rise to a jump in the bulk current. Those features are even more pronounced in Fig. 6(c), showing the corresponding solution for $\delta=0$, i.e., without any compact layer on the electrodes. The double-layer voltage remains low, so the bulk current is almost in phase with the driving voltage.

As discussed in the previous section, the very large capacitance of the diffuse layer predicted by PB theory is not realistic. For the solution in Fig. 6(c) the maximal ion concentration in the diffuse layer almost reaches 10^4 times the bulk concentration, which could easily trigger steric effects, even for a nominally dilute electrolyte. Figure 6(d) shows the result when such are taken into account with a bulk volume fraction $\nu=0.01$. The result is markedly different: when crowding sets in, the diffuse-layer capacitance drops and $\tilde{\zeta}$ grows rapidly with $\tilde{q}$. At lower charging, though, the system is still governed by dilute theory, so we still see a rapid shift in $\tilde{\zeta}$ with an associated jump in $\bar{J}$ when the double layer changes polarity.

C. Equivalent circuit

A useful concept for analyzing the cell response is an equivalent circuit diagram like that shown in Fig. 7(a). The transport through the bulk electrolyte is represented by an Ohmic resistor $2R=2$, and the charge accumulation in the double layer by a series coupling of two capacitors C_S and C_D,

$$\frac{1}{C} = \frac{1}{C_S} + \frac{1}{C_D}. \tag{66}$$

Here, $C_S=1/\delta$ is the capacitance of the compact (Stern) layer and $C_D=-d\tilde{q}/d\tilde{\zeta}$ is the differential capacitance of the diffuse (Debye) layer, given by [53,58,68,70]

$$C_D = \frac{|\sinh(\tilde{\zeta})|}{[1+2\nu\sinh^2(\tilde{\zeta}/2)]\sqrt{2\ln[1+2\nu\sinh^2(\tilde{\zeta}/2)]/\nu}}. \tag{67}$$

In the Debye-Hückel limit this reduces to $C_D=1$ and $C=1/(1+\delta)$. At higher voltages, PB theory predicts a dramatic increase of $C_D=\cosh(\tilde{\zeta}/2)$, to the extent that $C \approx 1/\delta$. According to MPB theory, the diffuse-layer capacitance becomes a *nonmonotonic* function of $\tilde{\zeta}$, where the initial increase is followed by a decrease as $C_D \approx 1/|\nu\tilde{q}| \approx 1/|2\nu\tilde{\zeta}|^{1/2}$ once steric exclusion sets in.

The equivalent circuit representation is useful for understanding and interpreting the system response. However, from an experimental point of view the overall cell impedance is a key property that can easily be measured with high accuracy, e.g., using a lock-in amplifier. We define the (half-) cell impedance Z as the ratio between the first Fourier components of the applied voltage and the resulting current,

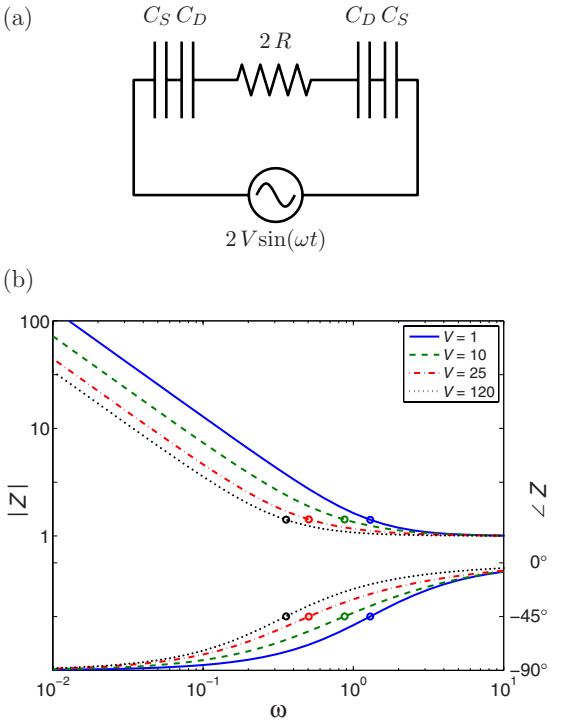

FIG. 7. (Color online) (a) Equivalent circuit representation for weakly nonlinear dynamics: compact and diffuse-layer capacitors in series with a bulk resistance. (b) Bode plot of the magnitude $|Z|$ and phase angle $\angle Z$ of the half-cell impedance for increasing driving voltage at $\delta=0.3$ and $\nu=0$. The characteristic frequency ω_o, where $\angle Z$ passes through $-45°$ and $|Z|$ bends up, is marked with circles.

$$Z = \frac{\int_0^T V_{\text{ext}}(t)e^{-i\omega t}dt}{\int_0^T \bar{J}(t)e^{-i\omega t}dt}. \tag{68}$$

Since the system is nonlinear, the impedance so defined is a function of both driving frequency and voltage. Figure 7(b) shows a Bode plot of the cell impedance Z for different values of V at $\delta=0.3$ and $\nu=0$. The curve shape is characteristic of an RC series coupling. At high frequency the Ohmic resistance of the bulk electrolyte dominates and $|Z|$ levels off at unity, while at low frequency the double-layer capacitance dominates and $|Z| \propto \omega^{-1}$. At the same time the phase angle $\angle Z$ drops from zero at high frequency to $-90°$ at low frequency. We define the *characteristic frequency* ω_o for a given driving voltage as that frequency where the phase angle passes through $-45°$, i.e.,

$$\angle Z(\omega_o) = -45°. \tag{69}$$

At this frequency the resistive and capacitive components contribute equally much to the overall cell impedance. Fig-

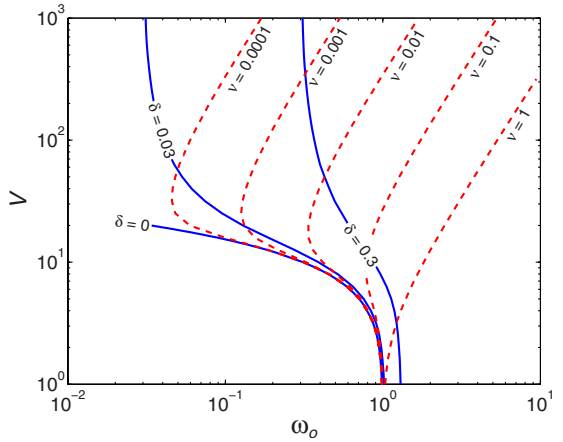

FIG. 8. (Color online) Characteristic frequency ω_o vs driving voltage, plotted for different values of δ with $\nu=0$ (solid line), and different values of ν with $\delta=0$ (dashed line).

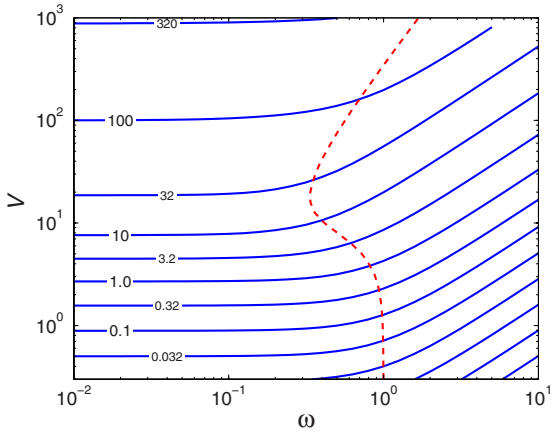

FIG. 9. (Color online) Contour plot of $\langle\tilde{w}\rangle$, the time-average excess salt concentration in the diffuse layer, as a function of driving frequency and voltage for $\delta=0$ and $\nu=0.01$. The dashed line marks the characteristic frequency ω_o.

ure 7(b) clearly shows that as the voltage is increased, the double-layer capacitance grows and the characteristic frequency shifts down.

The voltage dependence of ω_o is shown in more detail in Fig. 8, where ω_o is plotted versus V for different values of δ and ν. The GCS model simply predicts that ω_o should drop from $\omega_o=1+\delta$ at low voltage to $\omega_o\approx\delta$ at higher voltage. The same trend is seen for the BF model, up to the point where steric exclusion sets in; beyond this the double-layer capacitance decreases and ω_o increases, scaling as $\omega_o=O(\sqrt{\nu}V)$ at large voltages. These qualitative features predicted by our analysis may be interesting to compare to experimental impedance measurements at large ac voltages, below the threshold for Faradaic reactions or specific adsorption of ions, to seek evidence of steric effects in the liquid phase.

D. Neutral salt adsorption

In response to the ac driving, the diffuse layer periodically adsorbs and expels an excess amount of ions. At low voltage the charging comes about from both uptake of counterions and expulsion of coions, so the net salt adsorption is low, $\tilde{w}=\sqrt{\tilde{q}^2+4}-\sqrt{4}\approx\tilde{q}^2/4$ [cf. Eq. (57)] for $\tilde{q}\ll 1$. At higher voltage there are essentially no more coions to expel, so the charging process is dominated by uptake of counterions and $\tilde{w}\approx|\tilde{q}|$.

The excess amount of (counter)ions is taken up both from the adjacent diffusion layer *and* from that at the opposite electrode. In order to estimate when this effect starts to significantly perturb the concentration in the diffusion layer, it is necessary to know the time-average salt uptake $\langle\tilde{w}\rangle$. This is shown in Fig. 9 as a function of driving voltage and frequency for the BF model with $\delta=0$ and $\nu=0.01$. At low frequency, $\omega\ll\omega_o$, the double layer is almost fully charged, so that $\tilde{\Psi}\approx V_{\rm ext}$. At low voltage, $V\lesssim 1$, the figure shows that $\langle\tilde{w}\rangle\approx V^2/8$, while at high voltage, $V\gtrsim 30$, the steric effects dominate and $\langle\tilde{w}\rangle\approx\sqrt{V/\nu}$. For comparison, the GCS model predicts $\langle\tilde{w}\rangle\approx V/\delta$ in this limit, and the GC model $\langle\tilde{w}\rangle\approx\exp(V/2)$. At high frequency, $\omega\gg\omega_o$, the bulk resistance dominates the cell impedance, so $\bar{J}\approx V_{\rm ext}$ and $\tilde{q}=O(\bar{J}/\omega)$, from which the scaling is $\langle\tilde{w}\rangle\approx V^2/8\omega^2\lesssim 1$ or $\langle\tilde{w}\rangle\approx V/\omega\gtrsim 10$, depending on the level of charging.

E. Breakdown of weakly nonlinear dynamics

When an excess amount of salt $w=\epsilon\tilde{w}$ is adsorbed into the diffuse layer from a diffusion zone of width $\sqrt{\epsilon}$ or, more precisely $\sqrt{\epsilon/2\omega}$, it gives rise to a local $O(\epsilon\tilde{w}/\sqrt{\epsilon/2\omega})$ drop in the concentration. Hence, we expect the weakly nonlinear regime, characterized by fluctuations in the diffusion layer salt concentration being only a small perturbation to the bulk value, to break down for $\sqrt{2\epsilon\omega}\langle\tilde{w}\rangle=O(1)$. The critical voltage V_c for this to occur can be estimated by taking $|\tilde{q}|\approx\tilde{w}\approx 1/\sqrt{2\epsilon\omega}$ and $\bar{J}\approx i\omega\tilde{q}$ in Eq. (62) to get

$$V_c\approx\left|\frac{\delta}{\sqrt{2\epsilon\omega}}+\ln\left[\frac{2(e^{\nu/4\epsilon\omega}-1)}{\nu}\right]+i\sqrt{\frac{\omega}{2\epsilon}}\right|. \qquad (70)$$

For a typical microfluidic experiment with $c^*=1$ mM, $L=10$ μm, $\lambda_D=10$ nm, and $\lambda_S=3$ nm, corresponding to $\epsilon=0.001$ and $\delta=0.3$, and taking $\omega\approx 0.3$ (around 1 kHz in a KCl electrolyte), the critical voltage for breakdown of weakly nonlinear dynamics becomes $V_c\approx 18$ (or 460 mV) according to the GCS model; taking $\lambda_S=0$ nm and $a\approx 2$ nm, corresponding to $\delta=0$ and $\nu=0.01$, the BF model predicts $V_c=23$ (or 580 mV). (See Fig. 12 below for details of the frequency dependence.) For comparison, Bazant *et al.* estimated the critical voltage for a sudden dc voltage to $V_c\approx-\ln\epsilon\approx 7$ (or 175 mV) for the GC model and, similarly, Kilic *et al.* estimated $V_c\approx\nu/\epsilon\approx 10$ (or 250 mV) for the BF model.

F. Limit of ionic liquids

The absorption of neutral salt into the diffuse layers, and associated depletion of salt in the quasielectroneutral bulk diffusion layers, generally depends on the availability of space in the liquid (free of ions) for the total density of ions

to be much more concentrated in one region (the double layers) at the expense of another region (the diffusion layers). This is controlled in our MPNP model by the parameter $\nu=2a^3c^*=2c^*/c_{\max}$. In liquid electrolytes, ν represents the bulk volume fraction of (all) solvated ions, which is typically much less than 1 and even in saturated solutions of highly soluble ions would rarely exceed 0.1. As such, strongly nonlinear effects must generally be considered (below) in electrolytes at large applied voltages, especially in small systems.

The situation is different in ionic liquids or molten salts, which may be described by the limit $\nu\to 1$ in our MPNP model. This corresponds to the mean-field theory proposed by Kornyshev [70], where a value $\nu<1$ could model a somewhat lower volume fraction of the quasineutral bulk liquid phase, compared to the charged double layers, where strong normal electric fields may compress the counterions against a charged surface. In a molten salt, this density variation may be comparable to the expansion upon melting of an ionic crystal, which can be as large as 20%, so we might expect ν to be as small as 0.8, which is still much larger than for a typical electrolyte. This simple approach has had some success in describing experiments and simulations of simple ionic liquids [71,72], in what we would call a weakly nonlinear approximation, where the voltage-dependent quasiequilibrium double-layer capacitance is coupled to a constant bulk resistor.

An important prediction of our analysis is that this picture always remains valid up to large applied voltages for sufficiently large ν, so that ionic liquids can generally be described by the simple weakly nonlinear approximation. Using $V_c\approx\nu/\epsilon$ and noting that $\epsilon=\lambda_D/L\propto 1/\sqrt{c^*}\propto 1/\sqrt{\nu}$ (for fixed ion size and electrode separation) we find that the critical voltage for breakdown of weakly nonlinear *dynamics* grows with concentration like $V_c\propto\nu^{3/2}$. Likewise, Kilic *et al.* [54] estimated the critical voltage to significantly deplete the *steady-state* bulk salt concentration as $V_c\approx\nu/2\epsilon^2\propto\nu^2$. The basic picture is sketched Fig. 10: for concentrated electrolytes, the critical voltage rises steeply with ν, and in a molten salt, $\nu\approx 1$, the strongly nonlinear regime disappears and the nonlinear *RC* circuit approximation holds for all voltages.

The weakly nonlinear dynamics of ionic liquids in the MPNP model are not very different from those of concentrated electrolytes at large enough voltages to trigger steric effects in the double layer; see Figs. 5 and 8 where we have also included curves for $\nu=0.1$ and $\nu=1.0$.

V. STRONGLY NONLINEAR REGIME

The strongly nonlinear regime defined in Ref. [1] is characterized by significant $O(1)$ perturbations to the salt concentration in the quasineutral diffusion layers. From a physical point of view, this regime of the model is novel and interesting in several ways. It predicts the possibility of "capacitive desalination" of the bulk solution by an ac voltage, which is a remarkable example of rectification by nonlinearity, since even strong ac voltages are normally assumed not to perturb the bulk solution, in the absence of Faradaic reactions. This phenomenon may have interesting applications in microfluidics since ac voltages are often used to apply large electric fields without triggering reactions. Concentration gradients in the oscillating diffusion layers can become large enough to cause nearly complete depletion of salt just outside the double layer, causing it to lose its quasiequilibrium structure. This situation of "transient limiting current" is analyzed in the next section, but first we describe strongly nonlinear dynamics without diffusion limitation.

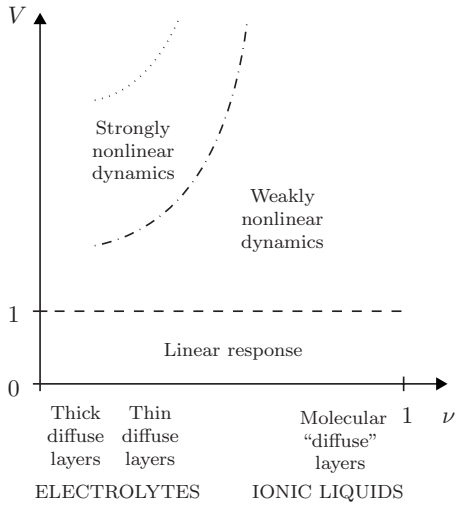

FIG. 10. Sketch of the different dynamical regimes for a blocking cell in the space of applied voltage V and nominal bulk volume fraction of ions, $\nu=2c^*/c_{\max}$. Linear response holds for $V\ll 1$ for any ν and diffuse-layer thickness $\epsilon=\lambda_D/L$. For thin diffuse layers ($\epsilon\ll 1$) in electrolytes ($\nu\ll 1$) there is a transition for $V>1$ to weakly nonlinear dynamics, where the diffuse layer acts as a voltage-dependent capacitor in series with a constant bulk resistance; at larger voltages, there is a transition to strongly nonlinear dynamics, which occurs first only with the oscillating diffusion layers (dashed-dotted line); at higher voltages there is another transition (dotted line) where the bulk solution becomes uniformly depleted by time-averaged mass transfer into the diffuse layers. The transition curves rise steeply with ν. For ionic liquids and the molten salt limit $\nu\approx 1$, only the weakly nonlinear regime is possible since there is not enough volume available to compress significant numbers of ions in the diffuse layers, which approach the molecular scale.

A. Dynamical response

Figure 11 shows the strongly nonlinear dynamic response at $V=30$, $\omega=0.3$, $\delta=0.3$, $\nu=0$, and $\epsilon=0.001$. First off we note that the qualitative difference against the weakly nonlinear solution from Fig. 6(b) is fairly small, even though the surface concentration $\hat{c}_s$ shows a significant variation. Quantitatively the largest difference is on the zeta potential, reaching 12% relative difference between the weakly and strongly nonlinear models. Perhaps this should not be too surprising: the surface concentration affects the double-layer charging dynamics only through the diffuse-layer charge-voltage relation [Eq. (52)] and only in a square-root dependence. Moreover, at this voltage the diffuse-layer capacitance is large enough that the compact layer dominates the overall response. Hence, for smaller values of δ, we should see a more significant difference between the weakly and strongly non-

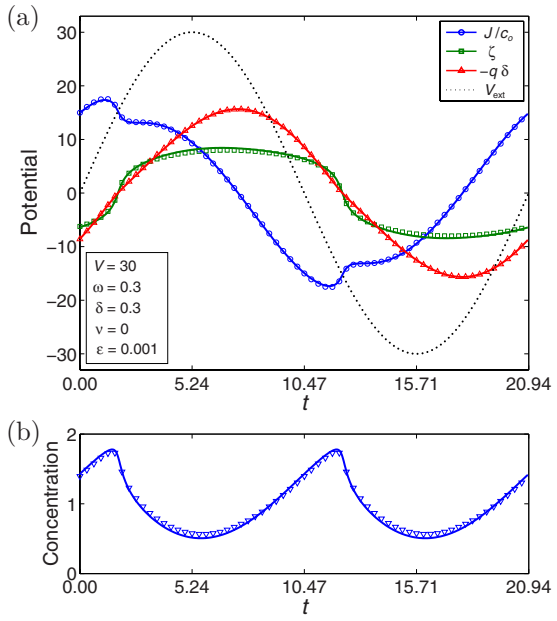

FIG. 11. (Color online) Strongly nonlinear response at $V=30$, $\omega=0.3$, $\delta=0.3$, $\nu=0$, and $\epsilon=0.001$. (a) Distribution of the cell voltage, $V_{\text{ext}}=\bar{J}/\bar{c}_o+\tilde{\zeta}-\tilde{q}\delta$ (dotted line), onto the bulk electrolyte, $\bar{J}/\bar{c}_o$ (circles), diffuse layer, $\tilde{\zeta}$ (squares), and compact layer, $-\tilde{q}\delta$ (triangles). (b) Concentration $\hat{c}_s$ at the inner edge of the diffusion layer. Symbols show results from the full numerical solution of the PNP equations, while the solid lines are predictions of our (much simpler) uniformly valid asymptotic approximations of Sec. III, which are seen to be in excellent agreement.

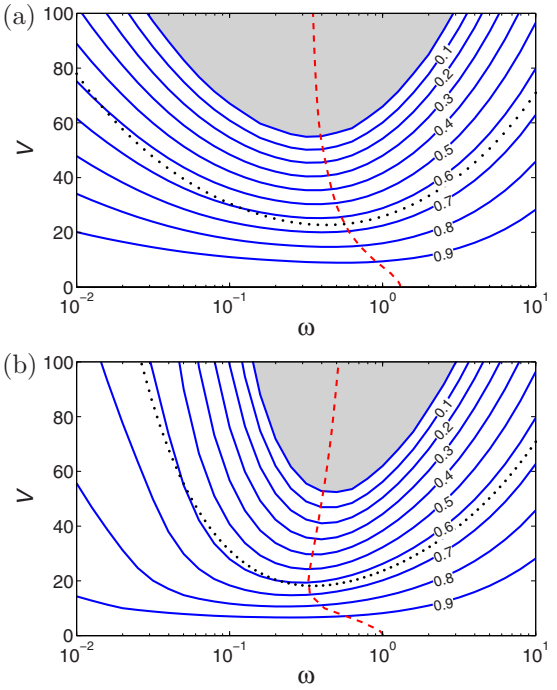

FIG. 12. (Color online) Contour plot of the minimal salt concentration $\min_t \hat{c}_s$ in the diffusion layer as a function of driving voltage and frequency for (a) $\delta=0.3$, $\nu=0$, and $\epsilon=0.001$; (b) $\delta=0$, $\nu=0.01$, and $\epsilon=0.001$. The dashed line marks the characteristic frequency ω_o, the dotted line marks the critical voltage V_c estimated by Eq. (70), and the shaded area marks a regime where $\min_t \hat{c}_s$ drops to zero and the double layer is driven out of quasiequilibrium. [For the lowest frequencies in the figure, the $O(\sqrt{\epsilon/2\omega})\approx 0.2$ wide diffusion layers extend across most of the bulk and no longer act as mathematical boundary layers.]

linear regimes. On the other hand, for $\nu\neq 0$ the double-layer voltage eventually becomes dominated by the condensed phase of ions developing at the steric limit, which scales as $|\tilde{\zeta}|\approx \nu\tilde{q}^2/2$ independent of $\hat{c}_s$.

B. Numerical validation

In order to test our uniformly valid asymptotic approximations above in the strongly nonlinear regime, we compare the results to the full numerical solution of the PNP model from Fig. 2. In Fig. 11 the solid lines show the results from the asymptotic analysis in Sec. III, and symbols show corresponding output from the full PNP model, determined in the following way: the compact-layer voltage $-\tilde{q}^{\text{PNP}}\delta$ is given directly by Eq. (21); the bulk current $\bar{J}^{\text{PNP}}$ and salt concentration $\bar{c}_o^{\text{PNP}}$ are evaluated at the center of the cell at $x=0$; the diffuse-layer voltage $\tilde{\zeta}^{\text{PNP}}$ is computed as the potential drop from the electrode surface at $y=0$ (i.e., $x=-1$) to a point immediately outside the diffuse layer, chosen (arbitrarily) at $y=3\epsilon$; and likewise the concentration $\hat{c}_s^{\text{PNP}}$ is evaluated at $y=3\epsilon$.

Overall, the agreement between the full PNP numerical solutions and the uniformly valid asymptotic approximations is excellent, in spite of the dramatic mathematical simplification at large voltages. The bulk current in the asymptotic model is slightly too small when $\hat{c}_s$ is maximal and slightly too large when $\hat{c}_s$ is minimal, with a maximal relative error of 1%, measured as $\max_t|\bar{J}-\bar{J}^{\text{PNP}}|/\max_t|\bar{J}^{\text{PNP}}|$. This small discrepancy is primarily due to our neglect of the change in conductivity in the diffusion layer and the associated (small) excess voltage [cf. Eq. (49)]. The compact-layer voltage agrees very well with the full numerical solution, whereas the diffuse-layer voltage $\tilde{\zeta}$ appears to be about 6% too large. However, even if the excess potential $\tilde{\psi}$ in the diffuse layer falls off exponentially at large $\tilde{y}$ [cf. Eq. (32)], measuring the diffuse-layer voltage in the PNP model only from $\tilde{y}=0$ to $\tilde{y}=3$, we miss a (small) fraction of the "true" result. Accounting for this, we find that the relative error is only 2%, mainly due to a phase lag between the two solutions. The same arguments apply to the salt concentration $\hat{c}_s$ at the inner edge of the diffusion layer: using Eq. (30) to compute $\tilde{c}$ at $\tilde{y}=3$ the agreement with the full numerical solution is accurate to within 1%, against 4% for the "raw" $\hat{c}_s$ data in Fig. 11(b).

C. Local salt depletion

In order to quantify the strength of the nonlinear response, we measure the minimal concentration in the diffusion layer over one period in time. For example, in Fig. 11(b) the minimal concentration is about $\min_t \hat{c}_s\approx 0.5$, which is attained just after $t=5.24$ and again after $t=15.71$. Figure 12 shows the result for $\min_t \hat{c}_s$ as a function of driving frequency and

voltage. Figure 12(a) shows the GCS model with $\delta=0.3$, $\nu=0$, and $\epsilon=0.001$, with at least two important points to note: first, for a given driving voltage, the salt depletion is most significant just around the characteristic frequency ω_o and, second, for a given driving frequency, $\min_t \hat{c}_s$ falls off roughly linearly with V.

The frequency dependence can be understood as follows: earlier we argued that when the diffuse layer adsorbs neutral salt from a diffusion layer of width $\sqrt{\epsilon/2\omega}$, the variations in $\hat{c}_s$ should scale as $\sqrt{2\epsilon\omega}\langle\tilde{w}\rangle$, which explains why the salt depletion becomes less significant at low frequency. On the other hand, the double layer only gets fully charged when the cell is driven below the characteristic frequency [cf. Fig. 9], so that overall we indeed expect to see the strongest salt depletion for $\omega\approx\omega_o$. The figure also displays the critical voltage V_c estimated by Eq. (70), and it is clear that this simple formula captures both the frequency dependence and appropriate voltage for $O(1)$ perturbations to arise in the diffusion layer.

Another important feature of the strongly nonlinear regime is the possibility of transient diffusion limitation. This occurs when the voltage is sufficiently large, and the frequency is sufficiently small, to temporarily, but completely, deplete the salt concentration at the inner edge of the diffusion layer. The shaded area in Fig. 12(a) marks the parameter range where $\min_t \hat{c}_s$ reaches zero, and the quasiequilibrium structure of the double layer breaks down. In this regime, we must revise our asymptotic analysis to produce uniformly valid approximations accounting for transient space-charge formation. This is the subject of Sec. VI below.

Volume constraints can have a significant effect on the strongly nonlinear dynamics of our model problem. Figure 12(b) shows the corresponding results for the BF model with $\delta=0$, $\nu=0.01$, and $\epsilon=0.001$. Again, the salt depletion is strongest when the system is driven around the characteristic frequency, although this has a different dependence on voltage, as noted above. Further it is clear that when steric exclusion sets in and the diffuse-layer capacitance decreases, the salt depletion becomes much less significant, especially at low frequency. This effect was noted by Kilic *et al.* [53,54] for the response to a sudden dc voltage, but its influence on strongly nonlinear ac response is more complicated. Crowding effects make the shaded area of transient diffusion limitation span a narrower range of frequencies, compared to the GCS model. However, in both models, the shaded area starts at roughly the same voltage (around $V\sim 55$) for the characteristic frequency.

VI. BREAKDOWN OF QUASIEQUILIBRIUM DOUBLE-LAYER STRUCTURE

As we have seen in Fig. 12, when the driving voltage is increased, the salt depletion in the diffusion layer becomes more and more pronounced, and at some point the minimal concentration can even drop to zero (within the shaded area). At that point, the quasiequilibrium structure of the double layer breaks down: the chemical potential diverges, and the effective width of the diffuse layer grows like $O(1/\sqrt{\hat{c}_s})$. Likewise, the quasielectroneutral solution in the diffusion layer breaks down when the concentration approaches zero: the leading-order charge density in the diffusion layer can be evaluated from the Poisson equation [cf. Eq. (50)],

$$\hat{\rho} = -\epsilon^{3/2}\frac{\bar{J}\partial_{\hat{y}}\hat{c}}{\hat{c}^2}. \tag{71}$$

At large voltage the flux into the double layer is dominated by uptake of counterions since there are no more coions to expel, so that at the inner edge we have $|\bar{J}|\approx\partial_{\hat{y}}\hat{c}/\sqrt{\epsilon}$ and $|\hat{\rho}|\approx\epsilon^2\bar{J}^2/\hat{c}^2$. Quasielectroneutrality in the diffusion layer remains a good approximation only as long as $\hat{c}\gg|\hat{\rho}|$ or

$$\hat{c}\gg|\epsilon\bar{J}|^{2/3}. \tag{72}$$

The breakdown of electroneutrality and concommitant expansion of the double layer into a nonequilibrium structure due to transient diffusion limitation, in the absence of any normal flux of ions at the electrodes, is a unique prediction of our model which we analyze in detail in this section.

A. Nonequilibrium double layer

The breakdown of quasiequilibrium in the double layer and of quasielectroneutrality in the bulk region is well known for electrochemical cells driven at a dc Faradaic current approaching the classical "limiting" current [45,48]. At the limiting dc current, the double layer acquires a steady nonequilibrium structure and expands in dimensionless width from $O(\epsilon)$ to $O(\epsilon^{2/3})$, as first described by Smyrl and Newman [46]. Rubinstein and Shtilman later showed that a "space-charge" region completely depleted of coions can develop at an electrode or ion exchange membrane when driven *above* the diffusion-limited current [47]. In this regime one can identify three sublayers within the nonequilibrium double layer, namely [48,50,51],

(i) An inner quasiequilibrium layer of width $O(\epsilon)$ at the electrode surface.

(ii) An extended space-charge layer of width $y_o > O(\epsilon^{2/3})$ that is completely depleted of coions.

(iii) A "Smyrl-Newman" transition layer of width $O(\epsilon^{2/3})$ around $y=y_o$ connecting the space-charge layer to the quasielectroneutral diffusion layer.

It is exactly the same nested boundary-layer structure that we see here develops in a cell driven dynamically at very large voltage even though the electrodes are blocking with no reactions taking place, and thus no normal flux of ions into or out of the cell. Instead, the double layer is driven out of equilibrium purely by nonlinear electrochemical relaxation within the cell, as counterions are adsorbed into the double layer so quickly and in such large numbers that bulk diffusion becomes *temporarily* rate limiting, within each ac period. We now develop uniformly valid asymptotic approximations for this regime.

1. Space-charge layer

When a negative voltage is applied on the left electrode, the space-charge layer developing is one completely depleted of anions, $\check{c}_-=0$ (denoting variables by a breve accent), while

the cation concentration is nonzero, $\check{c}_+ > 0$, but small. The ion transport is completely dominated by migration, and the flux is determined by the current fed into the boundary layers from the bulk,

$$\tfrac{1}{2}\check{c}_+ \partial_y \check{\phi} = |\bar{J}(t)|. \tag{73}$$

Substituting the Poisson equation $-\epsilon^2 \partial_y^2 \check{\phi} = \frac{1}{2}\check{c}_+$ and integrating, we get the leading-order field in the space-charge layer [50],

$$\partial_y \check{\phi} = \frac{1}{\epsilon}\sqrt{2|\bar{J}|(y_o - y)}, \tag{74}$$

where the integration constant $y_o(t)$ is born positive and equal to the width of the space-charge layer. The (small) charge density due to the counterions in the cationic space-charge layer is found by differentiation,

$$\check{\rho} = \frac{\check{c}_+}{2} = -\epsilon^2 \partial_y^2 \check{\phi} = \frac{\epsilon}{2}\sqrt{\frac{2|\bar{J}|}{y_o - y}}, \tag{75}$$

and the leading-order potential drop across the layer by integration,

$$\check{\Phi} = \check{\phi}(0) - \check{\phi}(y_o) = -\frac{2}{3\epsilon}\sqrt{2|\bar{J}|}\, y_o^{3/2}. \tag{76}$$

The analysis of the opposite case, where a positive voltage is applied on the electrode and a space-charge layer completely depleted of cations develops, is fully similar.

2. Inner diffuse layer

Within an $O(\epsilon)$ distance from the electrode surface, the counterions remain in quasiequilibrium with a constant electrochemical potential at leading order [50], i.e., for a space-charge layer completely depleted of anions

$$\tilde{\mu}_+ = \tilde{\phi} + \ln \tilde{c}_+ - \ln(1 - \nu\tilde{c}_+/2) = \text{const}, \tag{77}$$

from which the cation distribution is

$$\tilde{c}_+ = \frac{1}{\frac{\nu}{2} + e^{\tilde{\phi} - \tilde{\mu}_+}}. \tag{78}$$

Substituting into the Poisson equation and integrating, we find

$$\partial_{\tilde{y}}\tilde{\phi} = \sqrt{\kappa^2 + \frac{2}{\nu}\ln\left[1 + \frac{\nu}{2}e^{\tilde{\mu}_+ - \tilde{\phi}}\right]}, \tag{79}$$

where the integration constant κ is fixed as $\kappa = \sqrt{2|\bar{J}|y_o} = \epsilon\partial_y\check{\phi}(0)$ to match the field in the space-charge layer. The solution for the potential can be expressed in integral form as

$$\tilde{y} = \int_{\tilde{\phi}(0)}^{\tilde{\phi}(\tilde{y})} \frac{d\tilde{\phi}'}{\sqrt{\kappa^2 + \frac{2}{\nu}\ln\left[1 + \frac{\nu}{2}e^{\tilde{\mu}_+ - \tilde{\phi}'}\right]}}. \tag{80}$$

The difficulty is, however, that we cannot determine the chemical potential $\tilde{\mu}_+$ by matching with the space-charge layer because $\tilde{\phi} \to \infty$ and $\tilde{c}_+ \to 0$ for $\tilde{y} \to \infty$.

In the dilute limit $\tilde{c}_+ \ll 2/\nu$ the solution can be expressed in *closed* form [48,51]. Rewriting in terms of the excess potential $\tilde{\psi} = \tilde{\phi} - \check{\phi}$, we obtain

$$\tilde{\psi} = 2\ln[1 - (1 - e^{\tilde{\zeta}/2})e^{-\kappa\tilde{y}}], \tag{81}$$

where $\tilde{\zeta}$ is determined by the total charge $\tilde{q} = \partial_{\tilde{y}}\tilde{\phi}(0) = \partial_{\tilde{y}}\tilde{\psi}(0) + \kappa$ accumulated in the nonequilibrium double layer,

$$\tilde{\zeta} = -2\ln\left[\frac{1}{2} + \frac{\tilde{q}}{2\kappa}\right]. \tag{82}$$

Substituting Eq. (81) and $\tilde{c}_+ = -2\partial_{\tilde{y}}^2\tilde{\psi}$ into Eq. (77) we find

$$\tilde{\mu}_+ = \check{\phi}(0) + 2\ln(2\kappa) + \ln(1 - e^{\tilde{\zeta}/2}) \tag{83}$$

$$= \check{\phi}(0) + 2\ln(2\kappa) + \ln\left(\frac{\tilde{q} - \kappa}{\tilde{q} + \kappa}\right). \tag{84}$$

We note that for $\tilde{q} \gg \kappa$ the chemical potential approaches a level $\tilde{\mu}_+ = \check{\phi}(0) + 2\ln(2\kappa)$ that is independent of $\tilde{\zeta}$ or $\tilde{q}$ and determined only by the matching field from the space-charge layer.

Now, provided κ is much smaller than the field at the onset of steric exclusion, i.e., $\kappa \ll \sqrt{2/\nu}$, we can use Eq. (83) for the chemical potential also for the MPB problem. Substituting into Eq. (79) we then get

$$\tilde{q} = \sqrt{\kappa^2 + \frac{2}{\nu}\ln[1 + 2\nu\kappa^2(1 - e^{\tilde{\zeta}/2})e^{-\tilde{\zeta}}]}, \tag{85}$$

and, finally, solving for $\tilde{\zeta}$ and using $\kappa \ll \sqrt{2/\nu}$,

$$\tilde{\zeta} \simeq -2\ln\left[\frac{1}{2} + \frac{1}{2\kappa}\sqrt{2(e^{\nu\tilde{q}^2/2} - 1)/\nu}\right]. \tag{86}$$

3. Transition layer

The solution in the space-charge layer cannot be matched directly to the quasielectroneutral diffusion layer: the leading-order field from the space-charge layer is $O(\epsilon^{-1})$ but vanishes at $y = y_o$, whereas the field in the diffusion layer is $O(1)$ but diverges like $-\bar{J}/\hat{c} \approx 1/(y - y_o)$ [cf. Eqs. (48) and (74)]. In the transition zone for $|y - y_o| \le O(\epsilon^{2/3}/|\bar{J}|^{1/3})$ the field has a unique profile that can be expressed as [50]

$$\partial_y \phi = \frac{\bar{J}}{|\epsilon\bar{J}|^{2/3}}P(z), \tag{87}$$

where $P(z)$ is a Painlevé transcendent of the second kind and z is a rescaled spatial variable given by

$$z = \frac{|\bar{J}|(y - y_o) + \hat{c}_s}{|\epsilon\bar{J}|^{2/3}}. \tag{88}$$

See the Appendix for more details and a plot of $P(z)$. The voltage on this narrow layer is negligible in the overall cell response, but the solution does allow us to understand better both the spatial transition and the transition in time from quasiequilibrium to nonequilibrium structure.

4. Transition from quasiequilibrium to nonequilibrium

One challenging aspect in modeling the dynamics of the system is that (unlike the steady-state dc case analyzed in all prior work) it is not sufficient to have valid solutions for quasiequilibrium with $\hat{c}_s \gg |\epsilon\bar{J}|^{2/3}$ and nonequilibrium with $y_o \gg \epsilon^{2/3}/|\bar{J}|^{1/3}$. The dynamical response passes back and forth from quasiequilibrium to nonequilibrium, but the previous analysis of the inner diffuse layer from Secs. III C and VI A 2 breaks down in the transition regime from $\hat{c}_s = O(|\epsilon\bar{J}|^{2/3})$ to $y_o = O(\epsilon^{2/3}/|\bar{J}|^{1/3})$, leaving the diffuse-layer voltage from both Eqs. (54) and (86) divergent for $\hat{c}_s \to 0$ and $y_o \to 0$, respectively, at fixed $\tilde{q}$ and $\bar{J}$. This is problematic since the charge-voltage relation plays a central role in our dynamical model.

In order to resolve this, we have developed an approximate solution of the standard PNP equations for the inner diffuse layer that is uniformly valid in quasiequilibrium, nonequilibrium, and across the transition regime. Essentially, our approximation amounts to assuming constant, rather than variable, coefficients in the equation for the *excess* field in the boundary layer from the Painlevé II problem; see the Appendix for technical details. Then we obtain

$$\tilde{\psi} = 4\ \tanh^{-1}\left[\frac{\tanh(\tilde{\zeta}/4)e^{-\kappa\tilde{y}}}{1 - \frac{\breve{\kappa}}{\kappa}\tanh(\tilde{\zeta}/4)(1 - e^{-\kappa\tilde{y}})}\right], \tag{89}$$

where

$$\kappa = |\epsilon\bar{J}|^{1/3}\sqrt{3P(-z_o)^2/2 - z_o}, \tag{90}$$

$$\breve{\kappa} = |\epsilon\bar{J}|^{1/3}\mathrm{sgn}(\bar{J})P(-z_o), \tag{91}$$

$$z_o = (|\bar{J}|y_o - \hat{c}_s)/|\epsilon\bar{J}|^{2/3}, \tag{92}$$

and the charge-voltage relation is

$$\tilde{\zeta} = -2\ \ln\left(\sqrt{\left[\frac{\tilde{q} + \breve{\kappa}}{2(\kappa + \breve{\kappa})}\right]^2 + \frac{\kappa - \breve{\kappa}}{\kappa + \breve{\kappa}}} + \frac{\tilde{q} + \breve{\kappa}}{2(\kappa + \breve{\kappa})}\right). \tag{93}$$

The asymptotics of $P(z)$ are such that in the quasiequilibrium limit, where $\hat{c}_s \gg |\epsilon\bar{J}|^{2/3}$ and $z_o \ll -1$, we have $P(-z_o) \approx 1/z_o$, $\kappa \approx \sqrt{\hat{c}_s}$, $\breve{\kappa} \approx 0$, and we recover the standard Gouy-Chapman solution. In the nonequilibrium limit, where $y_o \gg \epsilon^{2/3}/|\bar{J}|^{1/3}$ and $z_o \gg 1$, we have $P(-z_o) \approx -\sqrt{2z_o}$, $\kappa \approx |\breve{\kappa}| \approx \sqrt{2|\bar{J}|y_o}$, and we recover the result from Eq. (82). Note also that Eq. (93) satisfies $\tilde{\zeta}(-\tilde{q}, \hat{c}_s, y_o, -\bar{J}) = -\tilde{\zeta}(\tilde{q}, \hat{c}_s, y_o, \bar{J})$.

In the limit $\bar{J} \to 0$ Eq. (93) displays a $\ln|\bar{J}|$ singularity for $y_o > 0$. However, transient diffusion limitation and formation of space-charge layers are essentially *driven* by the large (capacitive) current running into the double layer; hence, when the current diminishes, the neutral salt concentration profile spreads out by diffusion and rolls back the space-charge layer and eventually, when $\bar{J}$ approaches zero, the space-charge layer "collapses" and leaves behind a region of (low) neutral salt concentration. Therefore, the parameter range with $y_o > 0$ and $\mathrm{sgn}(\bar{J}\tilde{q}) > 0$ in Eq. (93) is not relevant in practice.

In the case when the bulk current changes sign suddenly, e.g., if the cell is driven by a square-wave rather than a harmonic voltage, the space-charge layer also collapses suddenly, with fast redistribution of ions in the former space-charge region. Since our analysis is based on quasi-steady-state in the space-charge and transition layers, it cannot describe the details of the response during such a sudden collapse.

5. Crowding effects

Extending our analysis to account for steric exclusion does not affect the space-charge layer since the concentration there is low. It does, however, affect the solution in the inner diffuse layer. Analytical progress is difficult for the MPNP equations, but noting that the MPB charge-voltage relations (54) and (86), both in quasiequilibrium and nonequilibrium, are obtained by substituting $\tilde{q}$ with $\mathrm{sgn}(\tilde{q})\sqrt{2(e^{\nu\tilde{q}^2/2} - 1)/\nu}$ in the corresponding PB results, we argue that the general MPB charge-voltage relation can be obtained similarly from Eq. (93), provided the field at the onset of steric exclusion is large enough, $\sqrt{2/\nu} \gg |\breve{\kappa}|$.

B. Modified diffusion layer

The width $y_o(t)$ of the space-charge layer is equal to the width of the region of complete salt depletion in the diffusion layer. In the quasielectroneutral part we still need to solve a simple diffusion problem,

$$\partial_t \hat{c} = \partial_{\hat{y}}^2 \hat{c}. \tag{94}$$

However, now it is to be solved on the dynamically changing interval $\hat{y} \in [\hat{y}_o(t), \infty)$, where $\hat{y}_o = y_o/\sqrt{\epsilon}$ is determined such that

$$\hat{y}_o(t) = 0 \quad \text{for } \hat{c}(0,t) > 0, \tag{95}$$

$$\hat{c}(\hat{y}_o(t), t) = 0 \quad \text{for } \hat{y}_o(t) > 0. \tag{96}$$

At the inner edge of the diffusion layer, the boundary condition is still obtained by matching with the salt flux out of the double layer,

$$-\frac{1}{\sqrt{\epsilon}}\lim_{\hat{y}\to\hat{y}_o^+}\partial_{\hat{y}}\hat{c} = \lim_{\hat{y}\to\hat{y}_o^+}\hat{F} \equiv \tilde{F}_o(t). \tag{97}$$

The problem can be solved using the method of images,

$$\hat{c} = \bar{c}_o + \sqrt{\epsilon}\int_0^T \frac{1}{2}[G_\omega(|\hat{y} - \hat{y}_o(t')|, t - t') + G_\omega(\hat{y} + \hat{y}_o(t'), t - t')]\tilde{F}_o(t')dt', \quad (98)$$

where the injection of flux at both $\pm\hat{y}_o(t')$ makes the origin act like a reflecting boundary, and the Green's function $G_\omega(\hat{y},t)$ is defined in Eq. (46). The definition of $\hat{y}_o$ through Eq. (96) ensures that $\hat{c}=0$ and $\partial_{\hat{y}}\hat{c}=0$ for $\hat{y}<\hat{y}_o(t)$ and, hence, using $\mp\partial_{\hat{y}}G_\omega(0^\pm,t)=\delta^+(t)$, the boundary condition (97) is indeed satisfied.

Interestingly, the modified diffusion layer does have a time-average excess salt content relative to the bulk: substituting Eq. (46) in Eq. (98) we find that

$$\langle\hat{c}\rangle = \bar{c}_o - \frac{\sqrt{\epsilon}}{2}\langle(|\hat{y} - \hat{y}_o| + |\hat{y} + \hat{y}_o|)\tilde{F}_o\rangle, \quad (99)$$

and hence the time-average excess amount of salt contained is

$$\sqrt{\epsilon}\int_0^\infty (\langle\hat{c}\rangle - \bar{c})d\hat{y} = -\frac{\epsilon}{2}\langle\hat{y}_o^2\tilde{F}_o\rangle, \quad (100)$$

where we used that $\langle\tilde{F}_o\rangle=-\langle\partial_t\tilde{w}\rangle=0$ [94]. Note that since $\tilde{F}_o$ is generally negative when $\hat{y}_o$ is nonzero, the excess salt content will be positive.

Since the local conductivity goes to zero when $\hat{c}$ vanishes at the inner edge, one might worry that the potential drop across the diffusion layer could be large. However, because the quasielectroneutral solution breaks down for $\hat{c}\lesssim|\epsilon\bar{J}|^{2/3}$, we find that the overall Ohmic potential drop across the quasielectroneutral diffusion layer is limited to $O(\ln|\epsilon\bar{J}|)$, which remains a small perturbation to that across the bulk electrolyte.

C. Model summary

Summarizing the model for the leading-order dynamic out-of-quasiequilibrium response, the charging of the double layer at the leftmost electrode is governed by

$$V_{\text{ext}} = \bar{J}/\bar{c}_o + \breve{\Phi} + \tilde{\zeta} - \tilde{q}\delta, \quad (101)$$

$$\partial_t\tilde{q} = -\bar{J}, \quad (102)$$

$$\tilde{w} = \sqrt{\tilde{q}^2 + 4\hat{c}_s} - \sqrt{4\hat{c}_s}, \quad (103)$$

$$\partial_t\tilde{w} = -\tilde{F}_o, \quad (104)$$

with the diffuse-layer and space-charge layer voltages, $\tilde{\zeta}$ and $\breve{\Phi}$, given by

$$\tilde{\zeta} = -2\ln\left(\sqrt{\left[\frac{\mathcal{Q}+\breve{\kappa}}{2(\kappa+\breve{\kappa})}\right]^2 + \frac{\kappa-\breve{\kappa}}{\kappa+\breve{\kappa}}} + \frac{\mathcal{Q}+\breve{\kappa}}{2(\kappa+\breve{\kappa})}\right), \quad (105)$$

$$\breve{\Phi} = \text{sgn}(\bar{J})\frac{2}{3\epsilon}\sqrt{2|\bar{J}|}y_o^{3/2}. \quad (106)$$

Here, $\mathcal{Q}=\text{sgn}(\tilde{q})\sqrt{2[\exp(\nu\tilde{q}^2/2)-1]/\nu}$ in the MPNP model, reducing to $\mathcal{Q}=\tilde{q}$ in the standard PNP model. The salt concentration $\hat{c}_s$ at the inner edge of the diffusion layer is determined from

$$\hat{c}_s = \bar{c}_o + \sqrt{\epsilon}\int_0^T \frac{1}{2}[G_\omega(|\hat{y}_o(t) - \hat{y}_o(t')|, t - t') + G_\omega(\hat{y}_o(t) + \hat{y}_o(t'), t - t')]\tilde{F}_o(t')dt', \quad (107)$$

and the width $y_o=\sqrt{\varepsilon}\hat{y}_o$ of the space-charge layer is determined from

$$\hat{c}_s y_o = 0, \quad \hat{c}_s \geq 0, \quad y_o \geq 0. \quad (108)$$

The parameters κ and $\breve{\kappa}$ are given by

$$\kappa = |\epsilon\bar{J}|^{1/3}\sqrt{3P(-z_o)^2/2 - z_o}, \quad (109)$$

$$\breve{\kappa} = \text{sgn}(\bar{J})|\epsilon\bar{J}|^{1/3}P(-z_o), \quad (110)$$

where $P(z)$ is the Painlevé transcendent and $z_o=(|\bar{J}|y_o-\hat{c}_s)/|\epsilon\bar{J}|^{2/3}$ is the rescaled position of the transition layer relative to the electrode. Finally, the bulk concentration is again determined by imposing global conservation of salt in the cell,

$$\bar{c}_o = 1 + \langle y_o^2\tilde{F}_o\rangle/2 - \epsilon\langle\tilde{w}\rangle. \quad (111)$$

We solve this problem numerically using a time-stepping algorithm. The major difficulty is to determine $y_o(t)$ in a self-consistent way, which we achieve using a bisection algorithm. More details are given in our supplementary material [93].

D. Dynamical response

Figure 13 shows the strongly nonlinear dynamic response at $V=120$, $\omega=0.3$, $\delta=0.3$, $\nu=0$, and $\epsilon=0.001$. In particular we note in Fig. 13(b) the appearance of a transient space-charge layer extending to a width of $y_o\lesssim0.04$, with an associated voltage $\breve{\Phi}$ in Fig. 13(a) that induces a visible drop in the bulk current $\bar{J}$.

In order to validate the asymptotic analysis we compare our results to the full numerical solution from Fig. 3, as shown with symbols in Fig. 13. Like in Sec. V B, the compact-layer voltage $-\tilde{q}^{\text{PNP}}\delta$ is given directly by Eq. (21), and the bulk current $\bar{J}^{\text{PNP}}$ and salt concentration $\bar{c}_o^{\text{PNP}}$ are evaluated at the center of the cell. The width y_o^{PNP} of the space-charge layer is taken (arbitrarily) as the largest region where either the cation or anion concentration drops below $\frac{1}{2}|\epsilon\bar{J}|^{2/3}$ and, finally, the concentration $\hat{c}_s^{\text{PNP}}$ and the overall voltage $(\tilde{\zeta}+\breve{\Phi})^{\text{PNP}}$ across the diffuse and space-charge layers are evaluated at the position $y_o^{\text{PNP}}+3\epsilon$.

The agreement between the asymptotic approximation and the full numerical solution is good, although the bulk

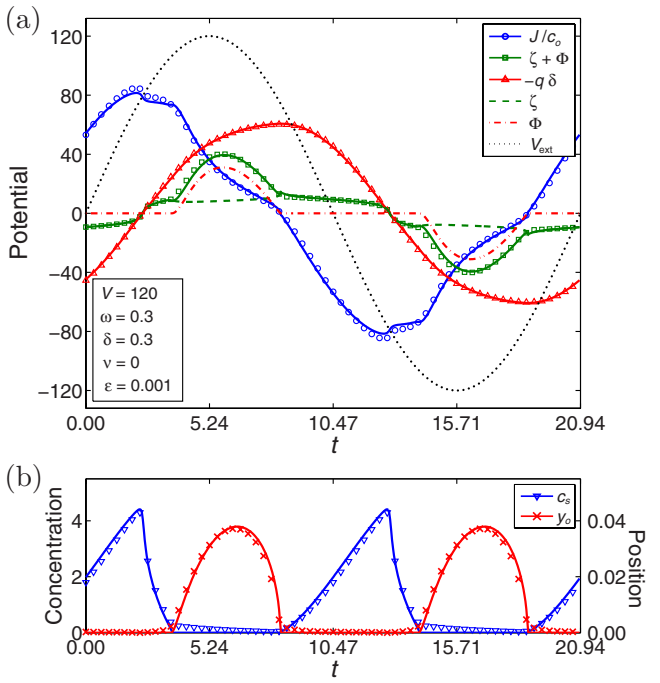

FIG. 13. (Color online) Strongly nonlinear response at $V=120$, $\omega=0.3$, $\delta=0.3$, $\nu=0$, and $\epsilon=0.001$. (a) Distribution of the cell voltage, $V_{\text{ext}}=\bar{J}/\bar{c}_o+\check{\Phi}+\tilde{\zeta}-\tilde{q}\delta$ (dotted line), onto the bulk electrolyte, $\bar{J}/\bar{c}_o$ (circles), diffuse layer (dashed line), space-charge layer (dashed-dotted line), and compact layer, $-\tilde{q}\delta$ (triangles); also shown is the sum of the space-charge and diffuse-layer voltages, $\tilde{\zeta}+\check{\Phi}$ (squares). (b) Concentration $\hat{c}_s$ at the inner edge of the diffusion layer (triangles) and extent y_o of space-charge layer (crosses). Solid and broken lines show results from our asymptotic model, and symbols show the full numerical solution of the PNP equations.

current $\bar{J}$ is visibly somewhat too low (by $\approx 5\%$) when $\hat{c}_s$ is large and too high when $\hat{c}_s$ is small. As before, part of the discrepancy on $\tilde{\zeta}$, $\check{\Phi}$, and $\hat{c}_s$ is due to the difficulty with defining the diffusion-layer inner edge on the full numerical solution, so it may be more appropriate to compare the full spatial profiles. We proceed to do that in the following section.

E. Uniformly valid approximations

So far we have been focusing on integral quantities such as the total charge and voltage, but the asymptotic analysis also predicts the full spatial profiles for the potential and ion concentrations in the cell: uniformly valid approximations in space are constructed by adding the inner and outer approximations and subtracting the overlaps [1,52]. In the absence of a space-charge layer the ion concentrations are given by

$$c_\pm(x,t)=\left[\tilde{c}_\pm\left(\frac{1+x}{\epsilon},t\right)-\hat{c}_s\right]+\hat{c}\left(\frac{1+x}{\sqrt{\epsilon}},t\right)-\bar{c}_o+\hat{c}\left(\frac{1-x}{\sqrt{\epsilon}},t\right)+\left[\tilde{c}_\mp\left(\frac{1-x}{\epsilon},t\right)-\hat{c}_s\right]. \tag{112}$$

In the presence of a space-charge layer, the challenge is to tie up the $O(\epsilon)$ but divergent counterion concentration in the space-charge layer [cf. Eq. (75)] with the $O(1)$ but vanishing concentration in the diffusion layer at $y=y_o$. The key is to employ the solution from the Smyrl-Newman transition layer: in the transition to the space-charge layer on the left electrode, the concentration can be written as

$$c_\pm=|\epsilon\bar{J}|^{2/3}[z+P^2/2\mp\operatorname{sgn}(\bar{J})\partial_z P], \tag{113}$$

as discussed in the Appendix. For $y\gg y_o$ this reduces to $c_+=c_-=(y-y_o)|\bar{J}|$, matching the flux $\partial_{\hat{y}}\hat{c}/\sqrt{\epsilon}\approx|\bar{J}|$ at the inner edge of the diffusion layer, whereas for $y\ll y_o$ the space-charge density in Eq. (75) is recovered. It is convenient to rewrite Eq. (113) as $c_\pm=\hat{c}+\check{\gamma}_\pm$, where $\check{\gamma}_\pm=c_\pm-\hat{c}$ is the excess concentration in the space-charge and transition layers relative to the diffusion layer, given by

$$\check{\gamma}_\pm=|\epsilon\bar{J}|^{2/3}[\min\{z,0\}+P^2/2\mp\operatorname{sgn}(\bar{J})\partial_z P]. \tag{114}$$

In linewith this, the excess concentration in the inner diffuse layer can be expressed as

$$\tilde{\gamma}_\pm=|\epsilon\bar{J}|^{2/3}[\tilde{R}^2/2+P\tilde{R}\mp\operatorname{sgn}(\bar{J})\partial_z\tilde{R}] \tag{115}$$

$$=(\partial_{\tilde{y}}\tilde{\psi})^2/2+\check{\kappa}\partial_{\tilde{y}}\tilde{\psi}\mp\partial_{\tilde{y}}^2\tilde{\psi}, \tag{116}$$

where $\tilde{R}=\operatorname{sgn}(\bar{J})\partial_z\tilde{\psi}=\operatorname{sgn}(\bar{J})\partial_{\tilde{y}}\tilde{\psi}/|\epsilon\bar{J}|^{1/3}$ is the (rescaled) inner excess field. Substituting $\tilde{\psi}$ from Eq. (89) we obtain the following lengthy expression:

$$\tilde{\gamma}_\pm=4\kappa^2\frac{2A-\check{\kappa}\sinh(\tilde{\zeta}/4)(Be^{\kappa\tilde{y}}-Ae^{-\kappa\tilde{y}}/B)}{[2\check{\kappa}\sinh(\tilde{\zeta}/4)+Be^{\kappa\tilde{y}}-Ae^{-\kappa\tilde{y}}/B]^2}\mp 4\kappa^2\frac{\kappa\sinh(\tilde{\zeta}/4)(Be^{\kappa\tilde{y}}+Ae^{-\kappa\tilde{y}}/B)}{[2\check{\kappa}\sinh(\tilde{\zeta}/4)+Be^{\kappa\tilde{y}}-Ae^{-\kappa\tilde{y}}/B]^2}, \tag{117}$$

where A and B are short-hands for $A=(\kappa^2-\check{\kappa}^2)\sinh^2(\tilde{\zeta}/4)$ and $B=\kappa\cosh(\tilde{\zeta}/4)-\check{\kappa}\sinh(\tilde{\zeta}/4)$. With this, the general form of (our approximation for) the ion distributions, uniformly valid in space and in time from quasiequilibrium, across the transition regime, to nonequilibrium, becomes

$$c_\pm(x,t)=\tilde{\gamma}_\pm\left(\frac{1+x}{\epsilon},t\right)+\check{\gamma}_\pm(z_+(t),t)+\hat{c}\left(\frac{1+x}{\sqrt{\epsilon}},t\right)-\bar{c}_o+\hat{c}\left(\frac{1-x}{\sqrt{\epsilon}},t\right)+\check{\gamma}_\mp(z_-(t),t)+\tilde{\gamma}_\mp\left(\frac{1-x}{\epsilon},t\right), \tag{118}$$

where $z_\pm(t)=\{|\bar{J}|[1\pm x\mp y_o(t)]\pm\hat{c}_s(t)\}/|\epsilon\bar{J}|^{2/3}$.

The resulting concentration profiles are shown in Fig. 14 for the solution at $V=120$, $\omega=0.3$, $\delta=0.3$, $\nu=0$, and $\epsilon=0.001$, displaying first injection of salt from the double layer into the diffusion layer, followed by reuptake in the double layer, salt depletion in the diffusion layer with formation and growth of an extended space-charge region, and—finally—collapse of the space-charge layer when the cell current changes direction. The figure also compares the uniformly valid approximation to the full numerical solution

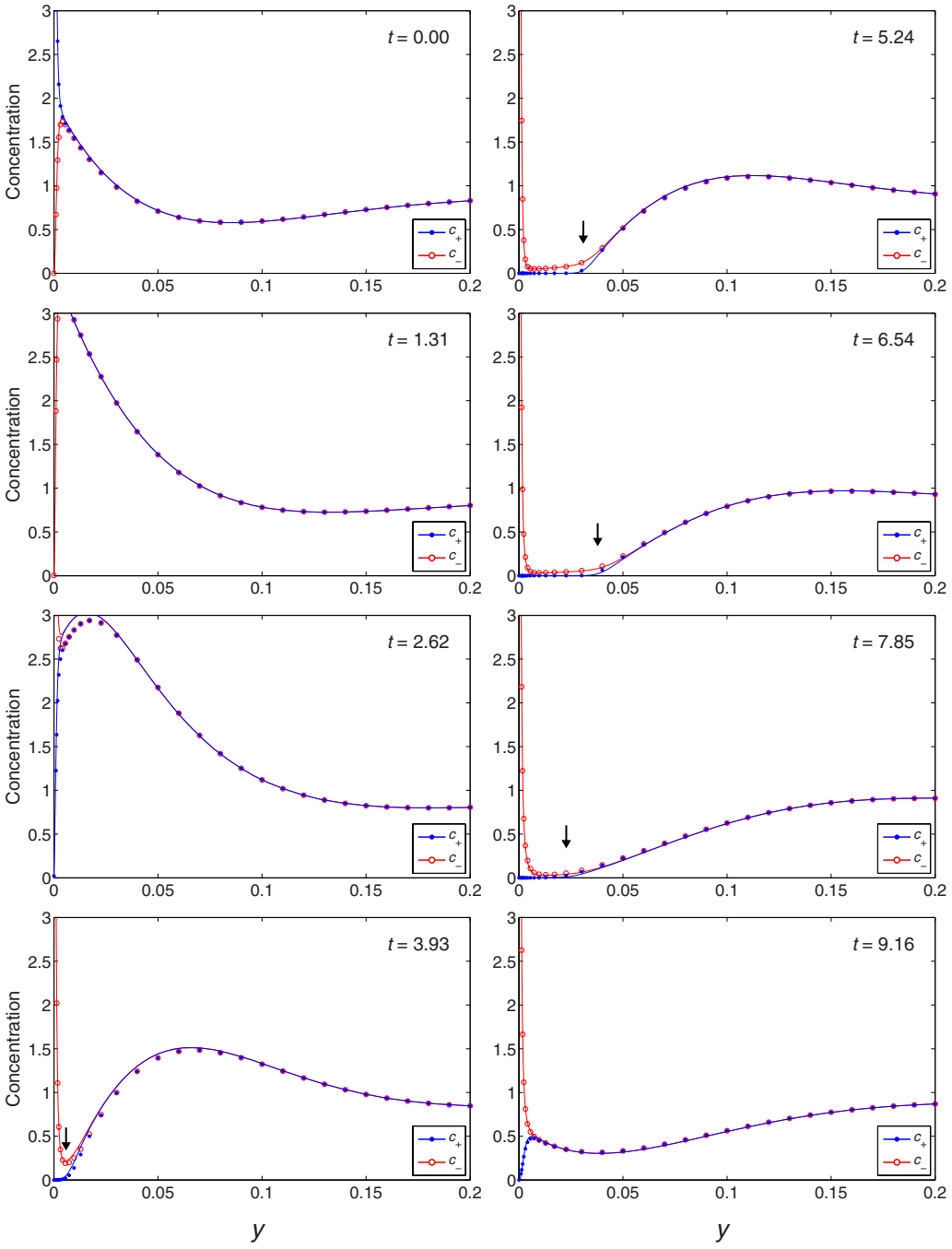

FIG. 14. (Color online) Concentration profiles at $V=120$, $\omega=0.3$, $\delta=0.3$, $\nu=0$, and $\epsilon=0.001$; "frames" cover one-half period in time starting from $t=0$. Open and filled circles show the cation and anion concentrations, respectively, according to the full numerical solution from Fig. 3, and solid lines show uniformly valid approximations based on the asymptotic analysis [Eq. (118)] with very good qualitative and quantitative agreement. Black arrows mark the extent $y_o(t)$ of the space-charge layer (if any) according to the asymptotic model.

from Fig. 3 and shows very good agreement. The relative error, measured as $\max_y\{\max_t|c_\pm - c_\pm^{\mathrm{PNP}}|/\max_t c_\pm^{\mathrm{PNP}}\}$, is below 5%.

F. Dominant voltage in double layer

For electrochemical cells running with a dc Faradaic current, it is well known that concentration polarization can play a dominant role at large voltage, with the space-charge layer determining the overall current-voltage relation for the system [47,48]. It is clear from Fig. 13 that, although $\breve{\Phi}$ is smaller than the compact-layer voltage $-\tilde{q}\delta$, it does affect the bulk current and slows down the charging process.

On the other hand, since $\breve{\Phi}$ depends on the capacitive current in ac, and since the diffuse-layer capacitance eventually drops when crowding starts to kick in, one might ask if the overall cell response will not be dominated by $\tilde{\zeta}$ at large voltage. Of course, that will depend on just how early the

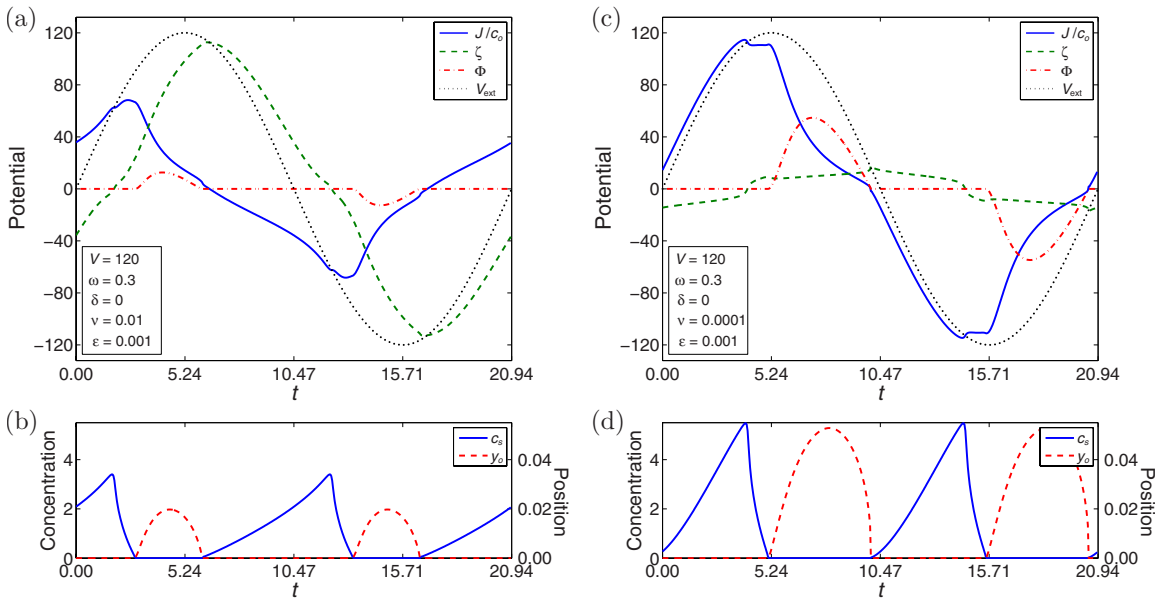

FIG. 15. (Color online) Strongly nonlinear response for MPB model with relatively large and small bulk ion volume fractions, ν =0.01 and 0.0001, respectively, at V=120, ω=0.3, δ=0, and ϵ=0.001. (a) and (c) Distribution of the cell voltage, $V_{\text{ext}}=\bar{J}/\bar{c}_o+\breve{\Phi}+\tilde{\zeta}$ (dotted line), onto the bulk electrolyte, $\bar{J}/\bar{c}_o$ (solid line), diffuse layer (dashed line), and space-charge layer (dashed-dotted line). (b) and (d) Concentration $\hat{c}_s$ at the inner edge of the diffusion layer (solid line) and extent y_o of space-charge layer (dashed line).

steric limit is reached, i.e., it depends on the nominal ion volume fraction ν.

Figure 15 shows the strongly nonlinear response for the MPB model with two different values of ν at V=120, ω =0.3, δ=0, and ϵ=0.001. In Figs. 15(a) and 15(b) where ν =0.01, the diffuse-layer voltage $\tilde{\zeta}$ dominates in the cell and the space-charge layer voltage $\breve{\Phi}$ is negligible. Also the bulk Ohmic potential drop $\bar{J}/\bar{c}_o$ is small because the driving frequency is below the characteristic frequency, $\omega<\omega_o$ (cf. Fig. 8). In Figs. 15(c) and 15(d), where ν=0.0001, the situation is the opposite: $\breve{\Phi}$ dominates over $\tilde{\zeta}$ in the nonequilibrium double layer, while $\bar{J}/\bar{c}_o$ dominates the overall cell response because this system is driven *above* the characteristic frequency, $\omega>\omega_o$.

The competition between $\breve{\Phi}$, $\tilde{\zeta}$, and $-\tilde{q}\delta$ is investigated further in Fig. 16, showing the peak values $\max_t \breve{\Phi}$, $\max_t \tilde{\zeta}$, and $\max_t \tilde{q}\delta$ as functions of driving voltage V in Figs. 16(a)–16(c) and frequency ω in Figs. 16(d)–16(f). Figures 16(a) and 16(d) show results for the PB model with δ=0.3, ν=0, and ϵ=0.001. Here, the compact-layer voltage dominates, although $\breve{\Phi}$ grows to a significant fraction at large voltages. Note in Fig. 16(d) that $\breve{\Phi}\propto|\bar{J}|^{1/2}y_o^{3/2}$ peaks around the characteristic frequency $\omega_o\approx 0.3$: at higher frequencies the double layer is not fully charged so $\tilde{w}$ and y_o decreases, while at lower frequencies it *is* fully charged and hence $\bar{J}$ decreases. Figures 16(b) and 16(e) show results for the MPB model with δ=0 and ν=0.01, where $\tilde{\zeta}$ completely dominates over $\breve{\Phi}$, whereas in Figs. 16(c) and 16(f) with ν=0.0001, $\breve{\Phi}$ dominates over $\tilde{\zeta}$ at large voltage and not-so-high frequency.

The relative magnitude of the double-layer voltages can be understood from a simple estimate: once steric effects dominate in the diffuse layer we have

$$\tilde{\zeta}=O(\nu\tilde{q}^2/2). \tag{119}$$

For the space-charge layer we have $\bar{J}=O(\omega\tilde{q})$ and y_o $=O(\epsilon\tilde{w})=O(\epsilon\tilde{q})$, so that

$$\breve{\Phi}=O(|\bar{J}|^{1/2}y_o^{3/2}/\epsilon)=O(\sqrt{\epsilon\omega}\tilde{q}^2). \tag{120}$$

This is an important finding: with both $\tilde{\zeta}$ and $\breve{\Phi}$ scaling as $O(\tilde{q}^2)$ at large voltage, we expect $\tilde{\zeta}$ to dominate over $\breve{\Phi}$ for $\nu\gg\sqrt{\epsilon\omega}$, i.e., in systems with high nominal concentration (large ν), large electrode separation (small ϵ), and at low frequency ($\omega\ll\omega_o$). Conversely, we expect $\breve{\Phi}$ to play a dominant role at large voltage for systems with very dilute electrolytes and small (micro)electrode geometry, driven around the characteristic (RC) frequency.

VII. SUMMARY AND DISCUSSION

We have developed a dynamical model for the response of dilute electrolytes to large applied ac voltages, building on a body of theoretical work on diffuse-charge dynamics for both the weakly and strongly nonlinear regimes [1,52,54], and on concentration polarization and space-charge layers in dc electrochemical systems running at steady-state conditions [47,48,50]. Our original contributions are the solution in the oscillating diffusion layer, controlling the extent of the transient space-charge layer and the uniformly valid formulation of the charge-voltage relation over the transition between quasiequilibrium and nonequilibrium.

We have compared our asymptotic analysis for the PNP model to a full numerical solution of the PNP equations and found good qualitative and quantitative agreement. The strongly nonlinear regime, characterized by strong concen-

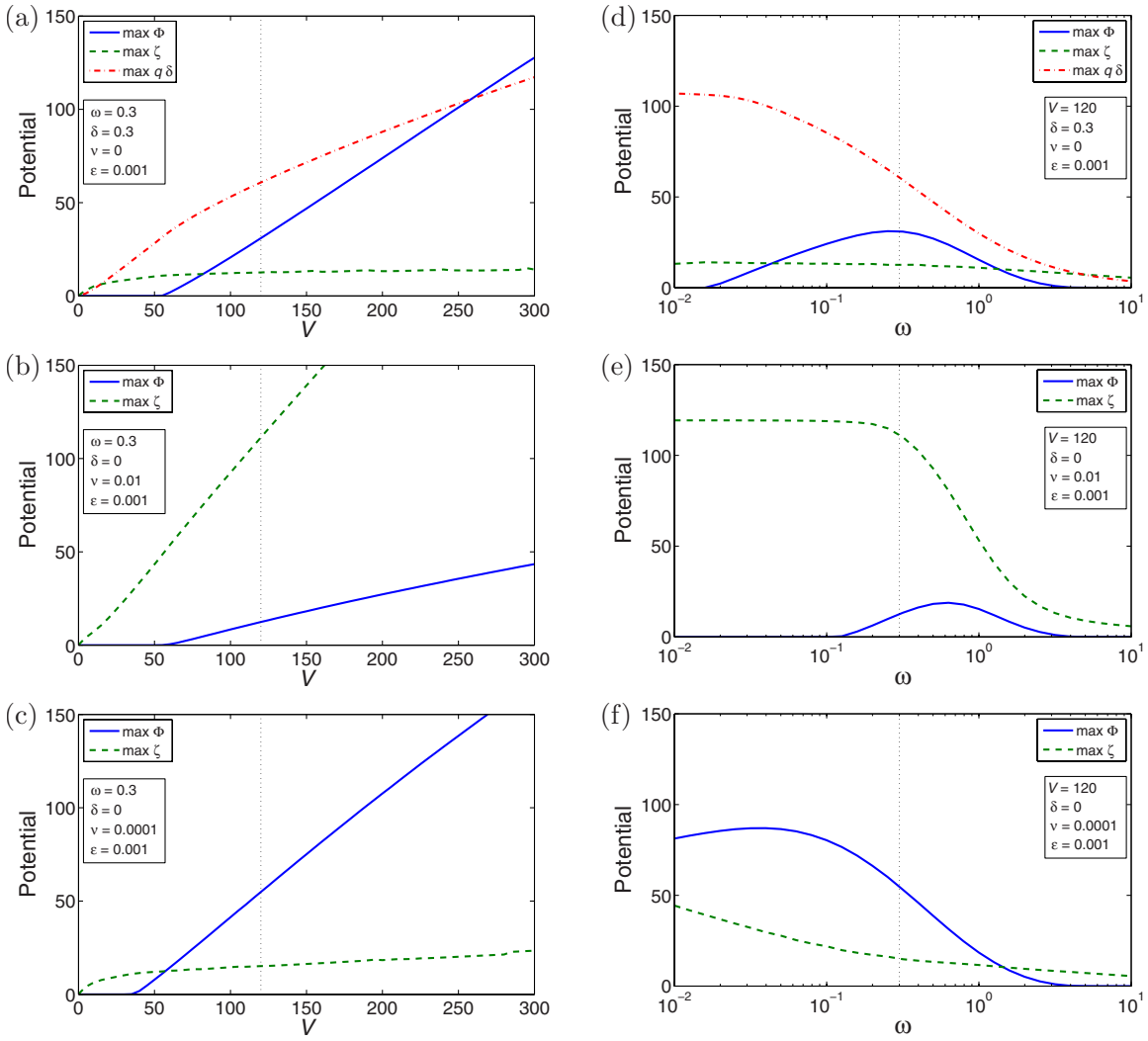

FIG. 16. (Color online) Peak voltages on space-charge layer, $\max_t \breve{\Phi}$ (solid line), diffuse layer, $\max_t \tilde{\zeta}$ (dashed line), and compact layer, $\max_t \tilde{q}\delta$ (dashed-dotted line), for different values of the capacitance ratio δ and nominal ion volume fraction ν. (a)–(c) show results at $\omega=0.3$ as a function of V, and (d)–(f) show results at $V=120$ as a function of ω. For the PB model, (a) and (d) show that the compact-layer voltage $-\tilde{q}\delta$ dominates at $\delta=0.3$, although $\breve{\Phi}$ becomes significant at large voltage. For the MPB model, (b) and (e) show that the diffuse-layer voltage $\tilde{\zeta}$ dominates at $\nu=0.01$, while in (c) and (f) the space-charge layer voltage $\breve{\Phi}$ dominates at $\nu=0.0001$.

tration gradients in the diffusion layer, sets in for $\sqrt{\epsilon\omega}\langle\tilde{w}\rangle = O(1)$, where the time-average excess salt concentration $\langle\tilde{w}\rangle$ depends not only on the driving frequency and voltage, but also on the intrinsic surface capacitance and crowding effects through δ and ν, respectively. At very large voltages we argue that the cell response should be dominated by space charge for $\nu \ll \sqrt{\epsilon\omega}$ and by crowding effects for $\nu \gg \sqrt{\epsilon\omega}$.

In particular, we find that for ionic liquids with $\nu=O(1)$, up to the molten salts limit $\nu \approx 1$, the strongly nonlinear regime disappears due to dominant crowding effects, which prevent the double layers from adsorbing significant numbers of ions from the bulk. The classical diffuse layer is effectively replaced with a molecular condensed layer. As a result, we justify the use of weakly nonlinear circuit models, as in Refs. [70–72], to describe the dynamics of ionic liquids up to very large time-dependent applied voltages.

Recently, Beunis *et al.* [55] presented an analysis of the *transient* response to a dc step voltage large enough to introduce transient space charge. They analyzed four extreme cases—the "double-layer limited" $(V \ll 1, \epsilon \ll 1)$, "diffusion limited" $(V \ll 1, \epsilon \gg 1)$, "geometry limited" $(V \gg 1, \epsilon \gg 1/\sqrt{V})$, and "space-charge limited" $(V \gg 1, \epsilon \ll 1/\sqrt{V})$—and developed closed form analytical solutions in each of those limits. In particular, for the space-charge-limited response, setting $\breve{\Phi}=V$ and $y_o=\epsilon|\tilde{q}|$, they predicted a characteristic $O(t^{-3/4})$ dependence in the bulk current, which they verified by experiments on a system with surfactant micelle charge carriers.

While the simple analytical results of Ref. [55] provides important insight to the *limiting* case when the space-charge layer completely dominates the response, our dynamical model is *uniformly* valid from small to very large voltages. The general applicability, however, comes at the expense that our strongly nonlinear model requires a set of integro-differential-algebraic equations to be solved numerically. In comparison, the weakly nonlinear "circuit" model, which ne-

glects any perturbations to the bulk and diffusion-layer electrolyte concentrations at leading order, can be formulated as a simple ordinary differential equation.

In many cases, even in dilute electrolytes, the nonlinear circuit model may actually give good account for *overall* current-voltage response of a cell, in particular when the double-layer capacitance is dominated by the compact layer or when crowding sets in and a condensed layer forms at the electrode. However, this does not necessarily mean that the weakly nonlinear analysis will account well for *all* aspects of the electrokinetic response, such as ac electro-osmotic fluid motion and pumping.

A. Two or more dimensions

The boundary-layer analysis can be easily extended to higher dimensions, provided the electrode geometry is smooth enough to be considered locally flat on the boundary-layer length scale. Then, the steady-state bulk response becomes

$$\boldsymbol{\nabla}\cdot\bar{\mathbf{J}}=0,\quad \boldsymbol{\nabla}\cdot\bar{\mathbf{F}}=0, \tag{121}$$

where $\bar{\mathbf{J}}=-\bar{c}\boldsymbol{\nabla}\bar{\phi}$ is the current, $\bar{\mathbf{F}}=-\boldsymbol{\nabla}\bar{c}+\mathrm{Pe}\langle\bar{\mathbf{u}}\rangle\bar{c}$ is the salt flux, and $\bar{c}=\bar{c}(\mathbf{r})$ is constant in time but not in space. The last term in the flux describes advection by the average fluid velocity $\langle\bar{\mathbf{u}}\rangle$; $\mathrm{Pe}=u_0L/D$ is the Péclet number, where $u_0=\varepsilon(kT/ze)^2/\eta L$ is the EO velocity scale and η is the dynamic viscosity. In the surface conservation laws, tangential flux through the highly charged diffuse layer must be taken into account [52,56,95–97], leading to

$$\partial_t\tilde{q}=-\mathbf{n}\cdot\bar{\mathbf{J}}-\epsilon\boldsymbol{\nabla}_s\cdot\tilde{\mathbf{J}}_s, \tag{122}$$

$$\partial_t\tilde{w}=-\tilde{F}_o-\epsilon\nabla_s\cdot\tilde{\mathbf{F}}_s, \tag{123}$$

where $\boldsymbol{\nabla}_s$ is the tangential gradient, and $\tilde{\mathbf{J}}_s$ and $\tilde{\mathbf{F}}_s$ are the surface excess current and salt flux, respectively, due to surface migration and EO convection. For the PB model it can be shown that

$$\tilde{\mathbf{J}}_s=(1+\mathrm{Pe})(\tilde{w}\boldsymbol{\nabla}_s\bar{\phi}+\tilde{q}\boldsymbol{\nabla}_s\ln\hat{c}_s), \tag{124}$$

$$\tilde{\mathbf{F}}_s=(1+\mathrm{Pe})(\tilde{q}\boldsymbol{\nabla}_s\bar{\phi}+\tilde{w}\boldsymbol{\nabla}_s\ln\hat{c}_s). \tag{125}$$

The same results would also apply for the MPB model if the concentration dependence of the ion mobility could be ignored in the highly crowded double layer [53], which is, however, not likely [58,97].

Assuming that transverse convection is weak enough, $\epsilon\,\mathrm{Pe}|\bar{\mathbf{u}}|\ll 1$, the diffusion layer can still be modeled by simple 1D diffusion in the normal direction, with the concentration given by Eq. (98). Matching with the steady solution in the bulk is then obtained by

$$\lim_{\hat{y}\to\infty}\hat{c}=\bar{c}_s-\sqrt{\epsilon}\hat{y}\mathbf{n}\cdot\bar{\mathbf{F}}, \tag{126}$$

$$\mathbf{n}\cdot\bar{\mathbf{F}}=\langle\tilde{F}_o\rangle=-\epsilon\langle\boldsymbol{\nabla}_s\cdot\tilde{\mathbf{F}}_s\rangle, \tag{127}$$

since the oscillating diffusion layer does not *accumulate* any salt on time average, but only acts as a buffer zone for the periodic flux in and out of the diffuse layer. In this way, surface conduction can drive bulk concentration gradients even in the steady-state response [52].

The bulk fluid motion is driven primarily by EO slip from the boundary layers. For the quasiequilibrium double layer, the effective tangential slip velocity according to PB theory becomes

$$\bar{\mathbf{u}}_s=\tilde{\zeta}\boldsymbol{\nabla}_s\bar{\phi}+4\ln[\cosh(\tilde{\zeta}/4)]\boldsymbol{\nabla}_s\ln\hat{c}_s. \tag{128}$$

For induced-charge electro-osmosis where both $\tilde{\zeta}$ and $\bar{\phi}$ depend on the external driving voltage, the velocity scales as $O(V^2)$ at low voltages [15,98]. At larger voltages, PB theory predicts stall of $\tilde{\zeta}$ and scaling only as $O(V\ln V)$ [11], whereas the MPB model predicts a return to the $O(V^2)$ scaling once crowding effects set in [69]. Or, this assumes that the viscosity in the highly crowded double layer is equal to the bulk value; if it is significantly reduced one might expect the velocity to scale as $O(V\ln\sqrt{2/\nu})$, where $\ln\sqrt{2/\nu}$ is the diffuse-layer voltage in the dilute part *outside* the condensed layer [57,58].

When the double layer is driven out of quasiequilibrium, it is still governed by surface conservation laws like Eqs. (122) and (123). The surface fluxes $\tilde{\mathbf{J}}_s$ and $\tilde{\mathbf{F}}_s$ are no longer given by Eqs. (124) and (125), but they should remain dominated by the inner diffuse layer since the concentration (and hence conductivity) in the space-charge layer is low.

If the space-charge layer does not contribute much to the surface flux, it plays a major role on EO fluid motion: the voltage $\breve{\Phi}$ drives a Smoluchowski-type slip velocity

$$\bar{\mathbf{u}}_s=\breve{\Phi}\boldsymbol{\nabla}_s\bar{\phi}, \tag{129}$$

for which Dukhin coined the term "electro-osmosis of the second kind" (EO2) to distinguish it from the quasiequilibrium response [99]. This phenomenon has been studied extensively in the context of nonlinear electrophoresis of conductive particles made from ion-exchanger material [99,100].

Since many ac electrokinetic experiments involve microelectrodes and applied voltages of a few volts [16,101–104], including investigations on ac electro-osmotic micropumps [12–14,105], and since our analysis has shown that this is enough to create strong concentration polarization and transient space charge around the electrodes, we believe that EO2 could be important for interpreting the experimental results.

Rubinstein and Zaltzman showed that EO2 renders linearly unstable the quiescent solution of concentration polarization on a planar perm-selective membrane running at dc, leading to spontaneous formation of vortex pairs that stir up the concentration profile in the diffusion layer, which in turn enables the passage of "superlimiting" current through the membrane [50,51]. Presumably, a similar instability could occur for transient space-charge layers, although the threshold voltage may depend on whether the space-charge layer voltage $\breve{\Phi}$ is dominating in the overall cell response or not.

B. Diffusive dynamics in the bulk

The transient response in the bulk, while the cell relaxes toward the steady-state periodic solution, or as arising from a slowly varying ac voltage amplitude $V_{\rm ext}=V(\bar{t})\sin(\omega t)+V_o(\bar{t})$, is governed by diffusive dynamics on the slow time scale $\bar{t}=\epsilon t$,

$$\partial_{\bar{t}}\bar{c} = -\boldsymbol{\nabla}\cdot\bar{\mathbf{F}} = \boldsymbol{\nabla}^2\bar{c} - \mathrm{Pe}\langle\bar{\mathbf{u}}\rangle\cdot\boldsymbol{\nabla}\bar{c}, \tag{130}$$

driven by the time-average flux into the double layer,

$$\mathbf{n}\cdot\bar{\mathbf{F}} = \partial_{\bar{t}}\langle y_o^2\tilde{F}_o/2 - \epsilon\tilde{w}\rangle - \epsilon\langle\boldsymbol{\nabla}_s\cdot\tilde{\mathbf{F}}_s\rangle. \tag{131}$$

Here, the time averages are taken on the RC time scale t, i.e., for each time step on the slow time scale, we require the periodic response of the boundary layers on the RC time scale to be determined.

C. Faradaic reactions and general electrolytes

Much interest on electrokinetics is of course associated with electrochemistry and reactions on electrodes that are not blocking but support the passage of a Faradaic current. Then the surface conservation laws are enriched by the injection of a Faradaic current $J_{\rm ext}$ at the electrode surface and an associated salt flux $F_{\rm ext}$.

Depending on the charge-transfer resistance and on the driving frequency and voltage, the Faradaic current may be small compared to the capacitive current in ac, or it may completely dominate the charging dynamics of the double layer. For reactions controlled by Butler-Volmer kinetics, where the reaction rate grows exponentially with (compact-layer) voltage, the latter should be the case at sufficiently large voltage. Of course, this implies that the RC time scale, formed by the bulk Ohmic resistance and double-layer capacitance, may not be appropriate for describing the system response.

Moreover, for many reactions it is not sufficient to assume a binary electrolyte since neutral reaction products also play an important role. The problem of the dynamic response for general electrolytes seems daunting and is a challenge even for the steady-state response [106].

ACKNOWLEDGMENTS

This work was supported in part by the U.S. National Science Foundation under Contract No. DMS-0707641 (MZB). The authors thank ESPCI for hospitality during our collaboration.

APPENDIX

The theory for nonequilibrium double layers was originally developed for electrochemical systems passing a dc current in steady state [41,42,46], with boundary conditions representing either normal flux of ions into a permeable electrodialysis membrane [47] or via Faradaic charge-transfer reactions at an electrode [48]. If we consider a cationic space-charge layer formed with negative voltage on the left electrode, the Nernst-Planck equations become

$$F_+ = -\partial_y c_+ - c_+\partial_y\phi = 2\bar{J} < 0, \tag{A1}$$

$$F_- = -\partial_y c_- + c_-\partial_y\phi = 0. \tag{A2}$$

For a dc electrochemical system, this holds across the entire cell. For an ac system driven at large voltage, this holds (approximately) in the inner diffuse, space-charge, and Smyrl-Newman transition layers because the charging process is dominated by uptake of counterions (cations) rather than expulsion of coions (anions), such that $|F_+| \gg |F_-|$. However, in the bulk region and in the diffusion layer we have primarily Ohmic transport and $F_+ \approx -F_- \approx \bar{J}$.

The PNP equations can be manipulated as follows: adding and subtracting Eqs. (A1) and (A2) we obtain

$$F = -\partial_y c + \rho E = \bar{J}, \tag{A3}$$

$$J = -\partial_y \rho - cE = \bar{J}, \tag{A4}$$

introducing the field $E=-\partial_y\phi$. Substituting the Poisson equation, $\rho=\epsilon^2\partial_y E$, into Eq. (A3) and integrating gives us

$$c = \frac{\epsilon^2}{2}E^2 + |\bar{J}|(y - y_o^*), \tag{A5}$$

and plugging this into Eq. (A4) the problem is finally reduced to a single master equation for the electric field,

$$\epsilon^2\partial_y^2 E - \tfrac{1}{2}\epsilon^2 E^3 - |\bar{J}|(y - y_o^*)E = |\bar{J}|. \tag{A6}$$

Here, y_o^* is an integration constant, equal to the width y_o of the space-charge layer for $y_o^*>0$, whereas for $y_o^*<0$ we interpret it as $y_o^*=-\hat{c}_s/|J|$ [48]. Rescaling with

$$E = \frac{|\bar{J}|^{1/3}}{\epsilon^{2/3}}P, \quad y - y_o^* = \frac{\epsilon^{2/3}}{|\bar{J}|^{1/3}}z, \tag{A7}$$

we then arrive at

$$\partial_z^2 P = \tfrac{1}{2}P^3 + zP + 1. \tag{A8}$$

This is an instance of the second-order ordinary differential equation with Painlevé property (i.e., all movable singularities are poles) defining the Painlevé transcendents of the second kind. The connection between steady dc current in electrochemical cells and Painlevé transcendents was first noted by Grafov and Chernenko [41,42]. Equation (A8) has a unique "transition layer" solution $P(z)$ with no poles on the real axis and the following asymptotic behavior:

$$P(z) = \begin{cases} -1/z + O(1/z^4) & \text{for } z \to +\infty \\ -\sqrt{-2z} + O(1/z) & \text{for } z \to -\infty. \end{cases} \tag{A9}$$

The detailed shape of $P(z)$ is shown in Fig. 17(a) and compared with the leading-order asymptotics. Figure 17(b) shows the potential variation

$$\phi(z) = -\int_0^z P(z')dz', \tag{A10}$$

and Fig. 17(c) displays the rescaled charge density

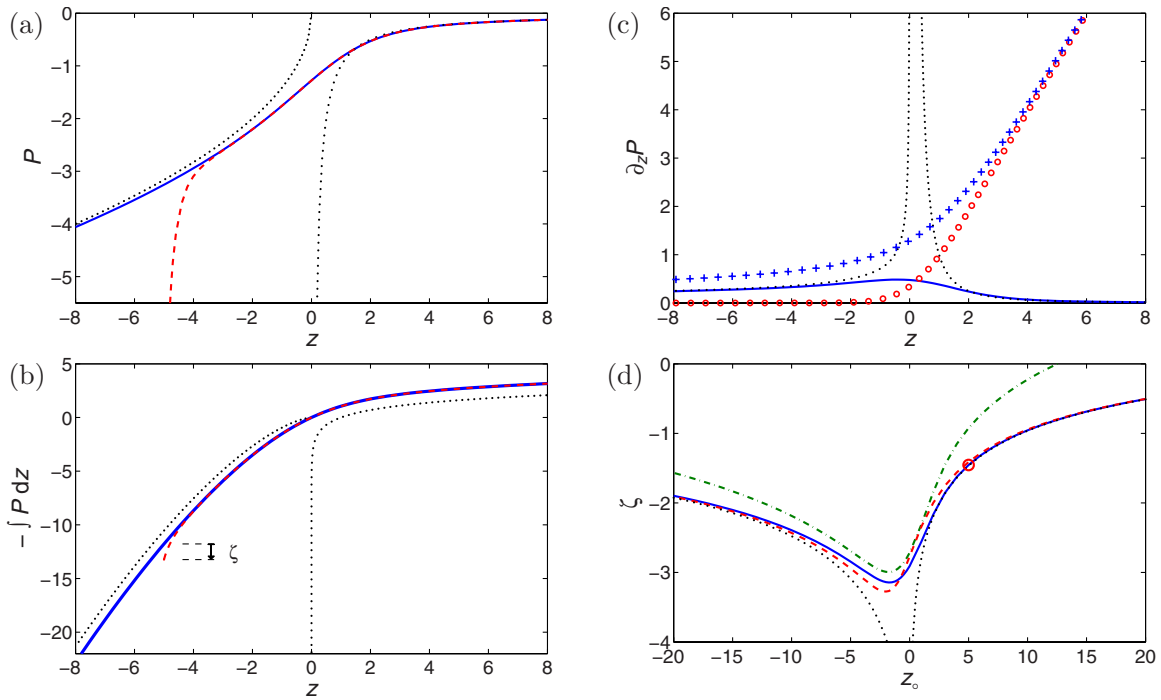

FIG. 17. (Color online) Solution in Smyrl-Newman transition layer in terms of Painlevé transcendents. (a) Rescaled electric field $P(z)$ (solid line) and leading-order terms from asymptotic approximation in the space-charge layer, $z \ll -1$, and diffusion layer, $z \gg 1$, (dotted line). The dashed line shows a solution $\tilde{P}$ to Eq. (A8) with b.c. $\tilde{P}=\tilde{P}_o=-10$ applied at $z=-z_o=-5$. (b) Potential variation $\phi=-\int_0^z P(z')dz'$ in transition layer (solid line), and leading-order asymptotics (dotted line). Again, the dashed line shows the result for the solution $\tilde{P}$. (c) Rescaled charge distribution $\partial_z P$ (solid line) and leading-order asymptotics (dotted line). Symbols show individual ion concentrations [cf. Eq. (A12)]. (d) Excess voltage $\tilde{\zeta}$ as a function of z_o with $\tilde{P}_o=-10$ (solid line), and leading-order terms from asymptotic approximation (dotted line). The circle marks $z_o=5$ corresponding to $\tilde{P}$ from (a) and (b), and the dashed and dashed-dotted lines show the approximation by Eqs. (A22) and (A27), respectively.

$$\frac{\rho}{|\epsilon\bar{J}|^{2/3}} = \partial_z P, \tag{A11}$$

and individual ion concentrations

$$\frac{c_\pm}{|\epsilon\bar{J}|^{2/3}} = z + \frac{1}{2}P^2 \pm \partial_z P. \tag{A12}$$

Boundary layer

The form of $P(z)$ describes the solution in the interior of the electrochemical cell. However, $P(z)$ generally does not satisfy the boundary conditions at the electrodes confining the cell. Imposing b.c.'s on the solution gives rise to boundary layers that can be understood mathematically as originating from poles in the solution, located outside the domain of the physical cell.

We focus on the behavior at the left electrode and consider a solution $\tilde{P}(z)$ to Eq. (A8) on the interval $z \in [-z_o, \infty)$, with boundary conditions $\tilde{P}(-z_o)=\tilde{P}_o$ and $\tilde{P}(\infty)=0$. Here,

$$-z_o = \frac{\hat{c}_s - |\bar{J}|y_o}{|\epsilon\bar{J}|^{2/3}} \tag{A13}$$

corresponds to the rescaled position of the electrode. Figure 17(a) shows the result for $z_o=5$ and $\tilde{P}_o=-10$: the excess field is rapidly screened out, and for $z \gtrsim -4$ we see that $\tilde{P}(z)$ follows $P(z)$ closely.

Let us introduce the excess field $\tilde{R}=\tilde{P}-P$ in the boundary layer. Substituting into Eq. (A8) we obtain

$$\partial_z^2 \tilde{R} = \tfrac{1}{2}\tilde{R}^3 + \tfrac{3}{2}P\tilde{R}^2 + k^2\tilde{R}, \tag{A14}$$

where $k=\sqrt{3P^2/2+z}$. Since the boundary layer is thin, it is reasonable to approximate the variable coefficients with constants $P_o=P(-z_o)$ and $k_o=\sqrt{3P_o^2/2-z_o}$ to get

$$\partial_z^2 \tilde{R} = \tfrac{1}{2}\tilde{R}^3 + \tfrac{3}{2}P_o\tilde{R}^2 + k_o^2\tilde{R}. \tag{A15}$$

This approximation is crudest for z_o close to zero, where the local screening length $1/k_o$ has a maximum; for $z_o \ll -1$ and $z_o \gg 1$ we have $k_o \approx \sqrt{-z_o}$ and $k_o \approx -P_o \approx \sqrt{2z_o}$, respectively.

Integrating twice on Eq. (A15) we obtain

$$\partial_z \tilde{R} = -\tilde{R}\sqrt{\tilde{R}^2/4 + P_o\tilde{R} + k_o^2}, \tag{A16}$$

$$z + z_o = \frac{1}{k_o}\left[\sinh^{-1}\left(\frac{P_o\tilde{R} + 2k_o^2}{|\tilde{R}|\sqrt{P_o^2/2 - z_o}} \right) - \sinh^{-1}\left(\frac{P_o\tilde{R}_o + 2k_o^2}{|\tilde{R}_o|\sqrt{P_o^2/2 - z_o}} \right) \right], \quad \text{(A17)}$$

from which

$$\tilde{R} = -\frac{2k_o^2}{P_o - \mathrm{sgn}(\tilde{R}_o)\sqrt{P_o^2/2 - z_o}\,\sinh[k_o(z + z^*)]}, \quad \text{(A18)}$$

where

$$z^* = z_o + \frac{1}{k_o}\sinh^{-1}\left(\frac{P_o\tilde{R}_o + 2k_o^2}{|\tilde{R}_o|\sqrt{P_o^2/2 - z_o}} \right). \quad \text{(A19)}$$

Finally, the excess potential $\tilde{\psi} = \tilde{\phi} - \phi$ is found by integrating $\tilde{R} = -\partial_z\tilde{\psi}$ to be

$$\tilde{\psi} = 4\tanh^{-1}\left[\frac{\tanh(\tilde{\zeta}/4)e^{-k_o(z+z_o)}}{1 + \frac{P_o}{k_o}\tanh(\tilde{\zeta}/4)[1 - e^{-k_o(z+z_o)}]} \right] \quad \text{(A20)}$$

$$= 2\ln\left[\frac{1 + \frac{k_o + P_o}{k_o - P_o}e^{\tilde{\zeta}/2} + (1 - e^{\tilde{\zeta}/2})e^{-k_o(z+z_o)}}{1 + \frac{k_o + P_o}{k_o - P_o}[e^{\tilde{\zeta}/2} + (1 - e^{\tilde{\zeta}/2})e^{-k_o(z+z_o)}]} \right]. \quad \text{(A21)}$$

Here, $\tilde{\zeta} = \tilde{\psi}(-z_o)$ is determined through the boundary condition $\tilde{P}_o = P_o + \tilde{R}_o$ as

$$\tilde{\zeta} = -2\ln\left(\sqrt{\left[\frac{\tilde{P}_o + P_o}{2(k_o - P_o)} \right]^2 + \frac{k_o + P_o}{k_o - P_o}} - \frac{\tilde{P}_o + P_o}{2(k_o - P_o)} \right) \quad \text{(A22)}$$

$$= 2\sinh^{-1}\left(\frac{\tilde{P}_o + P_o}{2\sqrt{k_o^2 - P_o^2}} \right) + \ln\left(\frac{k_o - P_o}{k_o + P_o} \right). \quad \text{(A23)}$$

Using $k_o \approx \sqrt{-z_o}$ and $P_o \approx 1/z_o$ for $z_o \ll -1$ it is easily verified that Eq. (A23) reduces to Chapman's formula,

$$\tilde{\zeta} \approx 2\sinh^{-1}\left(\frac{\tilde{P}_o}{2\sqrt{-z_o}} \right), \quad \text{(A24)}$$

in quasiequilibrium and, similarly, using $k_o \approx -P_o \approx \sqrt{2z_o}$ for $z_o \gg 1$ we find

$$\tilde{\zeta} \approx -2\ln\left(\frac{1}{2} - \frac{\tilde{P}_o}{\sqrt{8z_o}} \right), \quad \text{(A25)}$$

in accordance with Eq. (82) in nonequilibrium. However, while Eqs. (A24) and (A25) diverge for $z_o \to 0$ at fixed $\tilde{P}_o$, our general result (A22) only displays a local extremum. This is shown in Fig. 17(d) where $\tilde{\zeta}$ is plotted as function of z_o for $\tilde{P}_o = -10$. The figure also compares our result to the excess voltage from a direct numerical solution for $\tilde{P}$, and it is seen that Eq. (A22) slightly overestimates $\tilde{\zeta}$ for $z_o < 0$ and underestimates it for $z_o > 0$.

Singular transcendents

Zaltzman and Rubinstein [51] systematically studied the transition from quasiequilibrium to nonequilibrium by considering various ranges for the parameter z_o, solving appropriate approximations to the Painlevé equation in each range. In the transition regime they approximated the innermost part of the inner diffuse layer by an algebraically decaying solution, matched to a *singular* solution of the full original Painlevé equation (A8) in the outer part, writing

$$\tilde{P} \approx -\frac{2}{z + z_0 - 2/\tilde{P}_o} + \frac{2}{z + z_o} + P^\dagger(z; z_o). \quad \text{(A26)}$$

Here, $2/(z+z_o) + P^\dagger(z; z_o)$ is the *regular* part of a solution $P^\dagger(z; z_o)$ with a simple pole at $-z_o$, $P^\dagger(z; z_o) \sim -2/(z+z_o)$ for $z \to -z_o$, and $P^\dagger(\infty; z_o) = 0$. This allows them to write

$$\tilde{\zeta} = -2\ln(-\tilde{P}_o) + \varphi(z_o), \quad \text{(A27)}$$

where

$$\varphi(z_o) = \lim_{z\to\infty}\left[\int_{z_o}^{z} P^\dagger(z'; z_o) + \frac{2}{z' + z_o} - P(z')dz' - \ln(z + z_o) \right]. \quad \text{(A28)}$$

Their approximation is highly accurate for z_o in the transition range and large enough $\tilde{P}_o \ll -1$, and it is simple to evaluate once the function $\varphi(z_o)$ has been tabulated. For comparison, our result (A22) has a finite error for z_o in the transition range, an error that does not vanish at large $\tilde{P}_o$ but tends to a finite value, essentially being due to our approximation of the variable screening "constant" $k(z)$ in the tail of the excess field by a real constant k_o. On the other hand, our result matches fully with the quasiequilibrium and nonequilibrium limits, allowing us to use a single formulation of the charge-voltage relation for the entire dynamic solution procedure.

[1] M. Z. Bazant, K. Thornton, and A. Ajdari, Phys. Rev. E **70**, 021506 (2004).
[2] R. Kötz and M. Carlen, Electrochim. Acta **45**, 2483 (2000).
[3] J. H. Jang, S. Yoon, B. K. Ka, J. H. Jung, and S. M. Oh, J. Electrochem. Soc. **152**, A1418 (2005).
[4] M. Eikerling, A. A. Kornyshev, and E. Lust, J. Electrochem. Soc. **152**, E24 (2005).
[5] N. J. Dudney, J. B. Bates, D. Lubben, and F. X. Hart, in *Thin Film Solid Ionic Devices and Materials*, edited by J. Bates (The Electrochemical Society, Pennington, NJ, 1995), pp. 201–214.
[6] B. Wang, J. B. Bates, F. X. Hart, B. C. Sales, R. A. Zuhr, and J. D. Robertson, J. Electrochem. Soc. **143**, 3203 (1996).
[7] N. Takami, T. Ohsaki, H. Hasabe, and M. Yamamoto, J. Electrochem. Soc. **149**, A9 (2002).
[8] T. M. Squires and S. R. Quake, Rev. Mod. Phys. **77**, 977 (2005).
[9] A. Ramos, H. Morgan, N. G. Green, and A. Castellanos, J. Colloid Interface Sci. **217**, 420 (1999).
[10] A. Ajdari, Phys. Rev. E **61**, R45 (2000).
[11] L. H. Olesen, H. Bruus, and A. Ajdari, Phys. Rev. E **73**, 056313 (2006).
[12] V. Studer, A. Pépin, Y. Chen, and A. Ajdari, Analyst (Cambridge, U.K.) **129**, 944 (2004).
[13] J. P. Urbanski, J. A. Levitan, M. Z. Bazant, and T. Thorsen, Appl. Phys. Lett. **89**, 143508 (2006).
[14] M. M. Gregersen, L. H. Olesen, A. Brask, M. F. Hansen, and H. Bruus, Phys. Rev. E **76**, 056305 (2007).
[15] T. M. Squires and M. Z. Bazant, J. Fluid Mech. **509**, 217 (2004).
[16] J. A. Levitan, S. Devasenathipathy, V. Studer, Y. Ben, T. Thorsen, T. M. Squires, and M. Z. Bazant, Colloids Surf., A **267**, 122 (2005).
[17] B. P. Cahill, L. J. Heyderman, J. Gobrecht, and A. Stemmer, Phys. Rev. E **70**, 036305 (2004).
[18] A. Brask, D. Snakenborg, J. P. Kutter, and H. Bruus, Lab Chip **6**, 280 (2006).
[19] A. González, A. Ramos, H. Morgan, N. G. Green, and A. Castellanos, J. Fluid Mech. **564**, 415 (2006).
[20] J. Wu, M. Lian, and K. Yang, Appl. Phys. Lett. **90**, 234103 (2007).
[21] N. G. Green, A. Ramos, and H. Morgan, J. Phys. D **33**, 632 (2000).
[22] P. K. Wong, T. H. Wang, J. H. Deval, and C. M. Ho, IEEE/ASME Trans. Mechatron. **9**, 366 (2004).
[23] M. Z. Bazant and T. M. Squires, Phys. Rev. Lett. **92**, 066101 (2004).
[24] V. A. Murtsovkin, Colloid J. **58**, 341 (1996).
[25] T. M. Squires and M. Z. Bazant, J. Fluid Mech. **560**, 65 (2006).
[26] S. Gangwal, O. J. Cayre, M. Z. Bazant, and O. D. Velev, Phys. Rev. Lett. **100**, 058302 (2008).
[27] J. C. Weaver, J. Cell. Biochem. **51**, 426 (1993).
[28] J. C. Weaver and Y. A. Chizmadzhev, Biochemistry and Bioenergetics **41**, 135 (1996).
[29] H. Lu, M. A. Schmidt, and K. F. Jensen, Lab Chip **5**, 23 (2005).
[30] J. Voldman, Annu. Rev. Biomed. Eng. **8**, 425 (2006).
[31] J. Wu, Y. Ben, and H.-C. Chang, Microfluid. Nanofluid. **1**, 161 (2005).
[32] A. J. Bard, M. V. Mirkin, P. R. Unwin, and D. O. Wopf, J. Phys. Chem. **96**, 1861 (1992).
[33] K. Chen, J. Hirst, R. Camba, C. A. Bonagura, C. D. Stout, B. K. Burgess, and F. A. Armstrong, Nature (London) **405**, 814 (2000).
[34] B. Zhang, Y. H. Zhang, and H. S. White, Anal. Chem. **76**, 6229 (2004).
[35] M. L. A. Heien, A. S. Khan, J. L. Ariansen, J. F. Cheer, P. E. M. Phillips, K. M. Wassum, and R. M. Wightman, Proc. Natl. Acad. Sci. U.S.A. **102**, 10023 (2005).
[36] Q. Chi, O. Farver, and J. Ulstrup, Proc. Natl. Acad. Sci. U.S.A. **102**, 16203 (2005).
[37] A. J. Bard and L. R. Faulkner, *Electrochemical Methods* (John Wiley & Sons, Inc., New York, 2001).
[38] M. Sluyters-Rehbach and J. H. Sluyters, *Electroanalytical Chemistry* (Marcel Dekker, New York, 1970), Vol. 4, pp. 1–128.
[39] J. R. Macdonald, Electrochim. Acta **35**, 1483 (1990).
[40] L. A. Geddes, Ann. Biomed. Eng. **25**, 1 (1997).
[41] B. M. Grafov and A. A. Chernenko, Dokl. Akad. Nauk SSSR **146**, 135 (1962) [Sov. Phys. Dokl. **146**, 629 (1962)].
[42] A. A. Chernenko, Dokl. Akad. Nauk SSSR **153**, 1129 (1962) [Sov. Phys. Dokl. **153**, 1110 (1962)].
[43] J. Newman, Trans. Faraday Soc. **61**, 2229 (1965).
[44] A. D. MacGillivray, J. Chem. Phys. **48**, 2903 (1968).
[45] M. Z. Bazant, K. T. Chu, and B. J. Bayly, SIAM J. Appl. Math. **65**, 1463 (2005).
[46] W. H. Smyrl and J. Newman, Trans. Faraday Soc. **63**, 207 (1967).
[47] I. Rubinstein and L. Shtilman, J. Chem. Soc., Faraday Trans. 2 **75**, 231 (1979).
[48] K. T. Chu and M. Z. Bazant, SIAM J. Appl. Math. **65**, 1485 (2005).
[49] I. Rubinstein and B. Zaltzman, Phys. Rev. E **62**, 2238 (2000).
[50] I. Rubinstein and B. Zaltzman, Math. Models Meth. Appl. Sci. **11**, 263 (2001).
[51] B. Zaltzman and I. Rubinstein, J. Fluid Mech. **579**, 173 (2007).
[52] K. T. Chu and M. Z. Bazant, Phys. Rev. E **74**, 011501 (2006).
[53] M. S. Kilic, M. Z. Bazant, and A. Ajdari, Phys. Rev. E **75**, 021502 (2007).
[54] M. S. Kilic, M. Z. Bazant, and A. Ajdari, Phys. Rev. E **75**, 021503 (2007).
[55] F. Beunis, F. Strubbe, M. Marescaux, J. Beeckman, K. Neyts, and A. R. M. Verschueren, Phys. Rev. E **78**, 011502 (2008).
[56] K. T. Chu and M. Z. Bazant, J. Colloid Interface Sci. **315**, 319 (2007).
[57] M. Z. Bazant, M. S. Kilic, B. Storey, and A. Ajdari, New J. Phys. **11**, 075016 (2009).
[58] M. Z. Bazant, M. S. Kilic, B. Storey, and A. Ajdari, Adv. Colloid Interface Sci. **152**, 48 (2009).
[59] O. Stern, Z. Elektrochem. **30**, 508 (1924).
[60] J. J. Bikerman, Philos. Mag. **33**, 384 (1942).
[61] M. Dutta and S. N. Bagchi, Indian J. Phys. **24**, 2 (1950).
[62] S. N. Bagchi, J. Indian Chem. Soc. **27**, 199 (1950).
[63] M. Eigen and E. Wicke, Naturwiss. **38**, 453 (1951).
[64] M. Eigen and E. Wicke, J. Phys. Chem. **58**, 702 (1954).
[65] A. Iglic and V. Kralj-Iglic, J. Elec. Eng. Comput. Sci. **61**, 127 (1994).
[66] V. Kralj-Iglic and A. Iglic, J. Phys. II **6**, 477 (1996).

[67] I. Borukhov, D. Andelman, and H. Orland, Phys. Rev. Lett. **79**, 435 (1997).
[68] V. Freise, Z. Elektrochem. **56**, 822 (1952).
[69] B. D. Storey, L. R. Edwards, M. S. Kilic, and M. Z. Bazant, Phys. Rev. E **77**, 036317 (2008).
[70] A. A. Kornyshev, J. Phys. Chem. B **111**, 5545 (2007).
[71] M. V. Federov and A. A. Kornyshev, Electrochim. Acta **53**, 6835 (2008).
[72] M. V. Fedorov and A. A. Kornyshev, J. Phys. Chem. B **112**, 11868 (2008).
[73] K. B. Oldham, J. Electroanal. Chem. **613**, 131 (2008).
[74] P. M. Biesheuvel and M. van Soestbergen, J. Colloid Interface Sci. **316**, 490 (2007).
[75] L. H. Olesen, Ph.D. thesis, Technical University of Denmark, 2006; www.nanotech.dtu.dk/microfluidics
[76] Y. K. Suh and S. Kang, Phys. Rev. E **77**, 031504 (2008).
[77] Y. K. Suh and S. Kang, Phys. Rev. E **79**, 046309 (2009).
[78] S. J. Kim, Y. C. Wang, J. H. Lee, H. Jang, and J. Han, Phys. Rev. Lett. **99**, 044501 (2007).
[79] G. Yossifon and H.-C. Chang, Phys. Rev. Lett. **101**, 254501 (2008).
[80] S. R. de Groot and P. Mazur, *Non-equilibrium Thermodynamics* (Interscience Publishers, Inc., New York, 1962).
[81] R. Taylor and R. Krishna, *Multicomponent Mass Transfer* (John Wiley & Sons, Inc., New York, 1993).
[82] D. Antypov, M. C. Barbosa, and C. Holm, Phys. Rev. E **71**, 061106 (2005).
[83] A. A. Kornyshev and M. A. Vorotyntsev, Electrochim. Acta **26**, 303 (1981).
[84] A. Bonnefont, F. Argoul, and M. Bazant, J. Electroanal. Chem. **500**, 52 (2001).
[85] P. García-Sanchez, A. Ramos, N. G. Green, and H. Morgan, IEEE Trans. Dielectr. Electr. Insul. **13**, 670 (2006).
[86] J. O. Bockris and A. K. N. Reddy, *Modern Electrochemistry* (Plenum, New York, 1970).
[87] P. Delahay, *Double Layer and Electrode Kinetics* (Wiley, New York, 1965).
[88] A. A. Kornyshev, W. Schmickler, and M. A. Vorotyntsev, Phys. Rev. B **25**, 5244 (1982).
[89] B. B. Damaskin and V. A. Safonov, Electrochim. Acta **42**, 737 (1997).
[90] L. I. Daikhin, A. A. Kornyshev, and M. Urbakh, Phys. Rev. E **53**, 6192 (1996).
[91] L. I. Daikhin, A. A. Kornyshev, and M. Urbakh, Electrochim. Acta **42**, 2853 (1997).
[92] COMSOL MULTIPHYSICS, Comsol AB.
[93] See supplementary material at http://link.aps.org/supplemental/10.1103/PhysRevE.82.011501 for details on the numerical implementation and some MATLAB code.
[94] Equation (100) holds more generally when $\langle \tilde{F}_o \rangle \neq 0$, in steady state or for slow dynamics on the bulk diffusion time scale $\bar{t} = \epsilon t$, because $\mathbf{n} \cdot \nabla \bar{c} = -\mathbf{n} \cdot \bar{\mathbf{F}} = -\langle \tilde{F}_o \rangle$ [cf. Eq. (127)].
[95] J. J. Bikerman, Z. Phys. Chem. Abt. A **163**, 378 (1933).
[96] B. V. Deryagin and S. S. Dukhin, Colloid J. USSR **31**, 277 (1969).
[97] S. S. Dukhin, Adv. Colloid Interface Sci. **44**, 1 (1993).
[98] A. González, A. Ramos, N. G. Green, A. Castellanos, and H. Morgan, Phys. Rev. E **61**, 4019 (2000).
[99] S. S. Dukhin, Adv. Colloid Interface Sci. **35**, 173 (1991).
[100] Y. Ben, E. A. Demekhin, and H.-C. Chang, J. Colloid Interface Sci. **276**, 483 (2004).
[101] A. Ramos, H. Morgan, N. G. Green, and A. Castellanos, J. Phys. D **31**, 2338 (1998).
[102] N. G. Green, A. Ramos, A. González, H. Morgan, and A. Castellanos, Phys. Rev. E **61**, 4011 (2000).
[103] J. A. Fagan, P. J. Sides, and D. C. Prieve, Langmuir **21**, 1784 (2005).
[104] S.-C. Wang, Y.-W. Lai, Y. Ben, and H.-C. Chang, Ind. Eng. Chem. Res. **43**, 2902 (2004).
[105] A. B. D. Brown, C. G. Smith, and A. R. Rennie, Phys. Rev. E **63**, 016305 (2000).
[106] M. A.-K. Urtenov, E. V. Kirillova, N. M. Seidova, and V. V. Nikonenko, J. Phys. Chem. B **111**, 14208 (2007).